

Mirrorless lasing: a theoretical perspective

Aneesh Ramaswamy,¹ Jabir Chathanathil,² Dimitra Kanta,³ Emmanuel Klinger,^{3,4} Aram Papoyan,⁵ Svetlana Shmavonyan,⁵ Aleksandr Khanbekyan,⁵ Arne Wickenbrock,³ Dmitry Budker,^{3,6} and Svetlana A. Malinovskaya^{1,3}

¹*Department of Physics, Stevens Institute of Technology, Hoboken, NJ, USA*

²*DEVCOM Army Research Laboratory, Adelphi, MD, USA*

³*Helmholtz Institute Mainz, Johannes Gutenberg University, Mainz, Germany*

⁴*Université de Franche-Comté, SupMicroTech-ENSMM,*

UMR 6174 CNRS, Institut FEMTO-ST, Besançon, France

⁵*Institute for Physical Research, National Academy of Sciences of Armenia, Ashtarak-2, Armenia*

⁶*Department of Physics, University of California, Berkeley, CA, USA*

E-mail: aramasw1@stevens.edu

(Received September, 2023; revised September, 2023; accepted October, 2023)

Abstract- Mirrorless lasing has been a topic of particular interest for about a decade due to promising new horizons for quantum science and applications. In this work, we review first-principles theory that describes this phenomenon, and discuss degenerate mirrorless lasing in a vapor of Rb atoms, the mechanisms of amplification of light generated in the medium with population inversion between magnetic sublevels within the D_2 line, and challenges associated with experimental realization.

Keywords: Quantum Optics, Stimulated emission processes, Mirrorless lasing, Amplified spontaneous emission, Alkali vapors

I. INTRODUCTION

Over sixty years of existence, lasers (Light Amplification by Stimulated Emission of Radiation) have played a significant role in many areas of scientific research, industry and defense¹, continuously growing as new laser technologies are developed. There are three principal components usually attributed to a laser: a gain medium, a pumping process and a feedback loop². Lasing usually requires pumping the medium to a state of population inversion, although lasing without apparent inversion can occur in the case where quantum coherence is induced between lower levels³. There is a debate over whether lasing always requires a feedback loop. Lasing is often distinguished from processes such as Amplified Spontaneous Emission (ASE), Superradiance (SR) and Superfluorescence (SF)^{4,5}. Conventional lasers usually incorporate an optical resonator setup where mirrors are used to have light amplified over several round trips in the gain medium². In mirrorless lasing setups involving a feedback loop, the gain medium takes the role of the resonator – usually through multiple scattering processes⁴ – in systems with a range of disorder, including random lasers⁶ and distributed-feedback systems⁷. Lasing in gain medium with a nonresonant feedback loop provided by the same medium was considered by Letokhov⁸ who gave a theoretical treatment concerning light in the diffusive regime, see, for example, Ref.⁹. Disordered random media provide coherent feedback loops that generate lasing as seen in disordered ZnO nanoparticles in polycrystalline films¹⁰ and quantum-dot-doped liquid crystals¹¹. In random lasers, feedback is either resonant (phase sensitive, i.e. coherent) or non-resonant (frequency and phase independent, i.e. incoherent)¹⁰.

In this work, we adopt a broad definition of mirrorless lasing as directed monochromatic emission from an ensemble of atoms or molecules excited with pump laser light. The treatment of feedback loops arising from multiple scattering is not considered here. There is great interest in the phenomenon of mirrorless lasing in atomic vapors with theoretical^{3,12–19}, and experimental investigations^{20–25} conducted in both cold atoms and hot vapors. The problem of mirrorless lasing in atomic gases can be split into two: (*i*) the problem of the gain mechanism^{14,20} and (*ii*) the problem of multiple-scattering feedback mechanism^{4,16,17}. Mechanisms involving population inversion include Mollow gain (using a near-resonant strong pumping field), Raman gain (by driving transitions using off-resonance fields between two non-degenerate ground states, usually Zeeman or hyperfine levels), and parametric gain (us-

ing degenerate four-wave mixing (d-FWM) by way of counter-propagating pump fields)^{14,20}.

Experiments in alkali metal vapor have shown the presence of gain through the phenomenon of amplified spontaneous emission (ASE), see e.g.²⁶ and Refs. therein. The combination of ASE and d-FWM at above-threshold scatterer densities is suggested as a likely mechanism^{21,22}.

The present work covers theoretical fundamentals of the lasing mechanisms of a gas of atoms in free space, focuses on the phenomenon of amplification of spontaneous emission and discusses degenerate mirrorless lasing from a gas of alkali atoms with magnetically degenerate hyperfine states. We elucidate the mechanisms for mirrorless lasing in both forward and backward direction with respect to the pump laser beam and show that such process is possible even in the degenerate case of the directed light being of the same frequency as the pump. We reveal the role of population inversion among degenerate magnetic sublevels of the hyperfine manifolds on the light amplification. The paper is organized as follows. In Sec. II we present a first-principles theory describing mirrorless lasing and mechanisms of light amplification in a gas of atoms. In Sec. III we present a study of degenerate mirrorless lasing in rubidium vapor using a semiclassical approach. Finally in Sec. IV we review the current status of experimental investigation of degenerate mirrorless lasing followed by a summary.

II. FIRST-PRINCIPLES FORMALISM

We start with a microscopic approach for the problem of mirrorless lasing in a gas of atoms. A system of N multilevel atoms located in free space and driven by a classical pump field with envelope $E_p(t)$ and frequency ω_p is considered. Each atom A_i has momentum \mathbf{p}_i , center-of-mass (COM) position \mathbf{R}_i and relative position \mathbf{r}_i . We define the central potentials $V_i(R_i, r_i)$ and the atom-atom interactions mainly composed of the potentials, $W_{ij}(R_i, R_j, r_i)$, introduced by the repulsion between the electrons of atoms A_i and A_j respectively. The separation distance between any pair of atoms is in general much greater than the transition wavelength λ_p . Each atom A_i is travelling with COM velocity \mathbf{v}_i , such that transition frequencies and dipole moments are Doppler shifted. The dipole approximation is used such that the interaction with the classical field driving transition l for the i -th atom is given by $-\mu_{il}E_p(t)\cos(\omega_p t)(\sigma_{il}^+ + \sigma_{il}^-)$. The vacuum interaction is given by $g_{k;il}^{(\mu)}a_k^{(\mu)}\sigma_{il}^+ + \text{H.c.}$ We

define the Hamiltonians:

$$H_A = \sum_i \left(\frac{\mathbf{p}_i^2}{2m} + V_i(\vec{R}_i, \vec{r}_i) + \sum_{j \neq i} W_{ij}(\vec{R}_i, \vec{R}_j, \vec{r}_i) \right), \quad (1)$$

$$H_F = \frac{1}{8\pi} \int d^3r (|\mathbf{E}|^2 + |\mathbf{B}|^2), \quad (2)$$

$$H_{AL} = - \sum_{il} \mu_{il} E_p(\vec{R}_i, t) \cos(\omega_p t) \left[\sigma_l^+(\vec{R}_i) + \sigma_l^-(\vec{R}_i) \right], \quad (3)$$

$$H_{AF} = - \sum_{il} \int d^3k g_{\vec{k};il}^{(\mu)}(\vec{R}_i) a_{\vec{k}}^{(\mu)} \sigma_l^+(\vec{R}_i) + \text{H.c.} \quad (4)$$

From the above Hamiltonians, we determine the atomic density matrix equations and the Heisenberg equation of motion for the photon operator $\langle a_{\vec{k}}^{(\mu)\dagger} a_{\vec{k}}^{(\mu)} \rangle$ ¹⁹. We ignore the contribution from the exchange potential terms and we use the operator $U_L(t, t_1) = \exp\left\{-i \int_{t_1}^t H_{AL,I}(t')\right\} \exp\{-i(H_A + H_F)t\}$ to transform the system Hamiltonian to the field interaction reference frame where the atomic propagators are dressed with the pump field. This is to include the case where the system is continuously driven, as opposed to where the system is optically pumped and then left alone. The latter approach is often used in solid-state lasing gain media, where the presence of non-radiative emissions and quenching decrease the material radiative lifetimes²⁷. We note that there are separate, often competing²⁸, mechanisms for gain. A seed pulse can be continuously amplified by the system or ASE can be generated. We use the standard projection operator techniques to derive the time non-local Liouville-von-Neumann equation²⁹:

$$\begin{aligned} \frac{d}{dt} \rho_{A,I'} = & -i \left(\sum_{il} g_{\vec{k}i}^{(\mu)}(\vec{R}_i) \left[\sigma_{l,I'}^+(\vec{R}_i, t), \Omega^{0+}(\vec{R}_i, t) \right] + \text{H.c.} \right) \\ & + \sum_{ilm} \int_{t_0}^t dt' \left(\Gamma_{lm}(\vec{R}_i, t, t') \left[\hat{\sigma}_{l,I'}^+(\vec{R}_i, t), \hat{\sigma}_{m,I'}^-(\vec{R}_i, t') \rho_{A,I'}(t') \right] \right. \\ & \left. - \Gamma_{lm}(\vec{R}_i, t, t')^* \left[\hat{\sigma}_{l,I'}^-(\vec{R}_i, t), \rho_{A,I'}(t') \hat{\sigma}_{m,I'}^+(\vec{R}_i, t') \right] \right) \\ & - \sum_{il} \sum_{jm} \frac{1}{\hbar^2} \int_{t_0}^t dt' \left(\left[\hat{\sigma}_{l,I'}^+(\vec{R}_i, t), \hat{\sigma}_{m,I'}^-(\vec{R}_j, t') \xi_{m,l}^{(\mu'\mu)}(\vec{R}_j, \vec{R}_i, t', t) \right] \right. \\ & \left. - \left[\hat{\sigma}_{l,I'}^+(\vec{R}_i, t), \xi_{m,l}^{(\mu'\mu)}(\vec{R}_j, \vec{R}_i, t', t)^* \hat{\sigma}_{m,I'}^-(\vec{R}_j, t') \right] + \text{H.c.} \right), \end{aligned} \quad (5)$$

where $\Omega^{0+}(\vec{R}_i, t)$ is the vacuum Rabi field operator

$$\Omega^{0+}(\vec{R}_i, t) = \frac{1}{\hbar} \int d^3k \langle a_{\vec{k}}^{(\mu)} \rangle_F(t_0) e^{-i\omega_k t}, \quad (6)$$

$\Gamma_{lm}(\vec{R}_i, t, t')$ is the time-dependent correlator for the decay

$$\Gamma_{lm}^{(\mu)}(\vec{R}_i, t, t') = \int d^3k g_{\vec{k};l}^{(\mu)}(\vec{R}_i, t) g_{\vec{k};m}^{(\mu)*}(\vec{R}_i, t'), \quad (7)$$

and $\xi_{m,l}^{(\mu'\mu)}(\vec{R}_j, \vec{R}_i, t', t)$ represents stimulated emission processes driven by the quantum light fields

$$\xi_{m,l}^{(\mu'\mu)}(\vec{R}_j, \vec{R}_i, t', t) = \left\langle \left\{ \vec{d}_m^* \cdot \vec{E}^{(\mu')-}(\vec{R}_j, t') \right\} \left\{ \vec{d}_l \cdot \vec{E}^{(\mu)+}(\vec{R}_i, t) \right\} \right\rangle_F. \quad (8)$$

The first term in Eq. (5) is the Langevin force that depends on vacuum fluctuations. The second term is the spontaneous decay contribution and $\hat{\sigma}_l^\pm(\vec{R}_i, t)$ is the rotated dipole operator. Note that the time and position dependent exponential is included into the coupling rates. The final term is the stimulated absorption/emission term for a single atom, ($i = j$), and two-atom events, ($i \neq j$). The former provides a correction to spontaneous emission due to a non-zero quantum radiation field. We note that there is a dependence on the expectation value $\left\langle a_{\vec{k}}^{(\mu)\dagger*} a_{\vec{k}'}^{(\mu')} \right\rangle_F(t')$. In the case where the density matrix is separable, and $\vec{k} = \vec{k}'$ and $\mu = \mu'$, we get the product of the usual photon number operator and the atomic density matrix. When any of the last two conditions are not met, the final term represents a photonic coherence between two modes. The Heisenberg equations of motion for the photon number operator can be simply defined as

$$\left[\frac{1}{c} \frac{d}{dt} + i(\omega_k - \omega_{k'}) \right] \left\langle a_{\vec{k},I'}^{(\mu)\dagger}(t) a_{\vec{k}',I'}^{(\mu')}(t) \right\rangle(t) = S_s(t) + \mathcal{R}_s \left[\left\langle a_{\vec{k}/\vec{q},I'}^{(\mu)\dagger} a_{\vec{q}/\vec{k}',I'}^{(\mu')} \right\rangle(t) \right], \quad (9)$$

where $S_S(t)$ is the source term due to atomic spontaneous decay and $\mathcal{R}_s \left[\left\langle a_{\vec{k}/\vec{q},I'}^{(\mu)\dagger} a_{\vec{q}/\vec{k}',I'}^{(\mu')} \right\rangle(t) \right]$ represents scattering contributions involving other modes. Equations (5) and (9) are the microscopic equations required to model the time and space dependent atomic density matrix and quantum field equations. For optically thick systems with high disorder and/or non-ultracold temperatures, statistical averaging of the equations, including averaging over the position density and velocity distributions of atoms, and phase-space transforms are required to obtain macroscopic equations of motion³⁰.

A. The probe field gain

The most common method for generating an intense monochromatic beam is to amplify a weak probe pulse, $E_{pr}(t)$, using a medium which has undergone population inversion, in the dressed state basis, with respect to a transition having frequency close to the

probe frequency³¹. Additional methods involve using coherent fields to generate quantum interference between stimulated emission and absorption pathways to create gain without population inversion^{3,14,20,32}. The probe detuning, Δ_{pr} , the magnetic sub-level degeneracy, the presence of population inversion and the propagation direction of the pump beam(s) determine which amplification mechanism dominates.

A Hamiltonian analogous to that in Eq. (3) is used to model the atom-probe field interaction, which we call H_{pr} . We derive the rate equations for the probe field E_{pr} . Using the steady state absorption rate of quanta for a classical field³³, we write

$$\frac{\partial}{\partial t} E_{pr}(\vec{R}, t) = n(\vec{R}) \langle -i[H_{pr;I}(t), \rho_I(t)] \rangle \Delta(\vec{R}, \vec{r}_0), \quad (10)$$

where n is the density of atoms in the medium, and I denotes the field interaction picture associated with transformation $U_0(t, t_1) = \exp\{-i(H_A + H_F)t\}$. The terms in $H_{AL;I}(t)$ are restricted to atoms within a volume $\Delta(\vec{R}, \vec{r}_0)$ of radius \vec{r}_0 from the center \vec{R} .

To the first order in perturbation theory, the steady state of a driven atom results in absorption spectrum $g_A(\omega)$ of a weak probe field of mode M and frequency ω ³³

$$g_A(\omega) = \int_0^\infty d\tau e^{-i\omega\tau} [d_I^-(\tau), d_I^+(0)], \quad (11)$$

where $d_I^+(\tau)$ is the weighted sum of all dipole operators that correspond to transitions involving radiation of mode M :

$$d_I^+(\tau) = \sum_j (\hat{\epsilon} \cdot \vec{\mu}_j) \sigma_{j,I}^+(\tau). \quad (12)$$

The averaged single-atom absorption rate, $\alpha(\omega, t)$, of quanta of mode M and energy $\hbar\omega$ from a weak probe field with slowly varying amplitude $E_{pr}(t)$ and frequency ω according to³³ is

$$\alpha(\omega, t) = \langle g_A(\omega) \rangle \left| \frac{(\hat{\epsilon}_p \cdot \hat{d}_I) E_{pr}(t)}{\sqrt{2\hbar}} \right|^2. \quad (13)$$

Understanding of the scattering processes that contribute to stimulated emission of the probe field in the presence of strong driving pump fields requires a dressed state approach. In strong fields, the spectral state composition of the atoms is understood in terms of multi-photon dressed states $|\lambda_i, m\rangle$ with energies $E_i = \lambda_i + m\omega_p$. In this case, the unperturbed atomic dynamics at any time consists of ladder-type transitions between different m -number

states. Therefore, contributions to the stimulated emission of probe field photons must take into account these background ladder transitions³⁴.

The transition amplitudes for multi-photon processes can be found by looking at the diagrammatic expansion of the self-energy $\Sigma(t, t_0)$ ³⁵. This follows from the below form of the Liouville-von-Neumann equation:

$$\dot{\rho}_I(t) = \int_{t_0}^t dt' \rho_I(t') \Sigma(t', t). \quad (14)$$

For example, the sum of transition amplitudes for all three-photon processes that involve absorption of two pump photons and emission of one single probe photon is given by summing over three-vertex Keldysh diagrams with vertices $(t_1, \sigma_j^+ E_P^-)$, $(t_2, \sigma_l^- E_{pr}^+)$, $(t, \sigma_j^+ E_P^-)$. The vertices can be on the forward or backwards branch of the density matrix, and we sum over all permutations of the vertices.

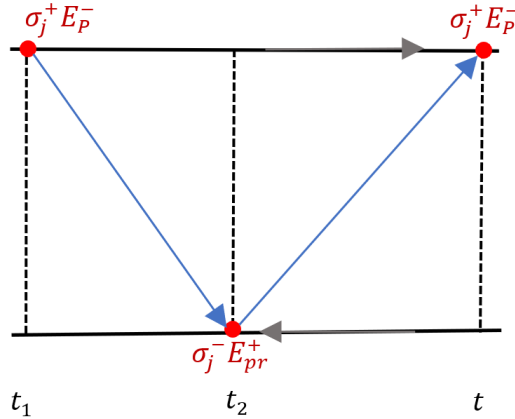


FIG. 1: A diagram representing the three-photon scattering process.

For the three-photon scattering process involving absorption of two pump photons and emission of one single probe photon, the contribution to the evolution of the atomic density matrix is given by

$$\begin{aligned} \delta^{(3)} \rho_{A,I}(t_1) &= \frac{E_P^2 E_{pr}}{\hbar^3} \int_0^t \int_0^{t_2} dt_1 dt_2 e^{-i((\Delta_P)(t+t_1) - \Delta_{pr} t_2)} \\ &\times \left[d_P^+ U(t, t_2) d_{pr}^- U(t_2, t_1) d_P^+ \rho_{A,I}(t_1) U^\dagger(t, t_1) \right. \\ &\left. + U(t, t_1) \rho_{A,I}(t_1) d_P^+(t_2) U^\dagger(t_2, t_1) d_{pr}^- U^\dagger(t, t_2) d_P^+(t) + \dots \right], \end{aligned} \quad (15)$$

where suspension points refer to all other possible time and branch (forward or reverse of the density matrix) orderings of the three vertices, see Fig. 1. The contribution in the

steady state limit is determined by substituting the steady state expression $\bar{\rho}_{A,I;s} = \bar{\rho}_{A,I;0} + \sum_j \bar{\rho}_{A,I;j} e^{-i\nu_j t}$. To look at the contribution for a specific transition, we compute the change in energy of the probe field, $\langle H_p \hat{X} \rangle$, for the particular transition described by the string of operators, \hat{X} .

In the following subsections, we described possible gain mechanisms using the example of a two-level degenerate system modeling the $F = 2 \rightarrow F = 3$ component of $^{87}\text{Rb } D_2$ transition.

B. Mollow gain

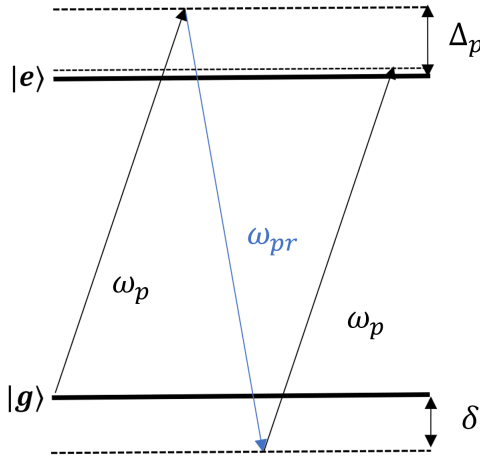


FIG. 2: Mollow gain in a two-level system (TLS). The pump field (ω_p), with detuning Δ_p , pumps atoms into the higher energy state. Depending on the sign of Δ_p , the probe field with frequency ω_{pr} inducing two-photon detuning δ is either amplified or reduced due to a three-photon scattering process. The probe field polarization is parallel to the polarization of the pump field.

In the case where the probe field is near two-photon resonance, Mollow gain³³ dominates with the gain mechanism due to a three-photon process involving the absorption of two pump photons and stimulated emission of a probe photon²⁰, see Fig. 2. Population inversion in the dressed state basis occurs here and results in gain/loss in the sidebands around the resonance peak in the absorption spectrum³⁶.

Figure 3 shows the absorption spectrum for the case of the resonant driving field. Note that, in this work, frequency parameters (such as $\Delta_{p,pr}$) and the excited state decay rate are expressed in units of Γ , and time parameters in the units of $1/\Gamma$. The feature seen

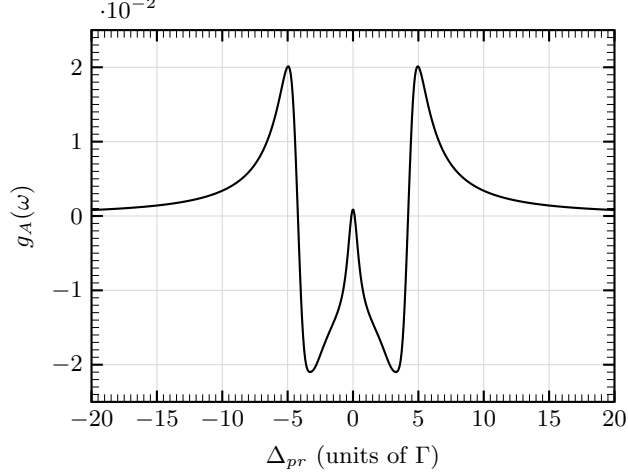


FIG. 3: Absorption spectrum of light with parallel (to pump) polarization for the resonantly driven ^{87}Rb system with parameters $\Gamma = 1.0$, $\Omega_p = 4\Gamma$, $\Delta_p = 0$.

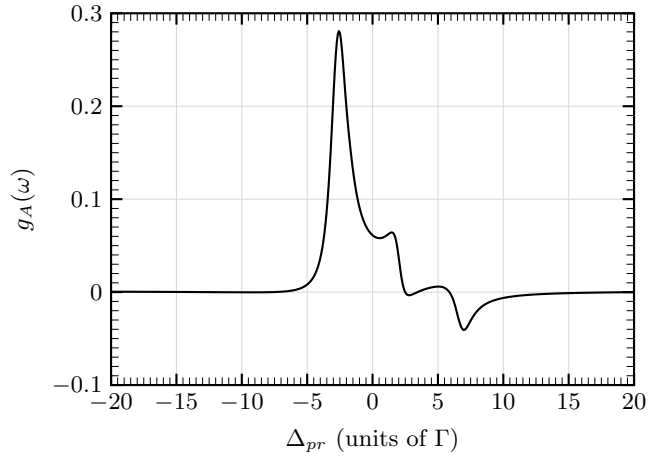


FIG. 4: Absorption spectrum of light with parallel (to pump) polarization for the off-resonantly driven ^{87}Rb system with parameters $\Gamma = 1.0$, $\Omega_p = 4\Gamma$, $\Delta_p = 2\Gamma$

around $\Delta_{pr} = 0$ corresponds to an interference between multiple two-photon processes. The dominant resonant contribution is the two-photon Rayleigh scattering process involving an absorption of the probe photon and spontaneous emission of a photon having the same frequency³⁷. Additionally there are processes involving absorption of a pump photon and emission of a probe photon and vice versa. The greatest gain components are observed at the sidebands centered at the dressed state frequencies $\pm\Omega_p$ in the resonant driving case. Increasing Δ_p from zero, results in an asymmetric spectrum where amplification occurs only on one sideband while an absorption feature occurs on the other, as shown in Fig. 4.

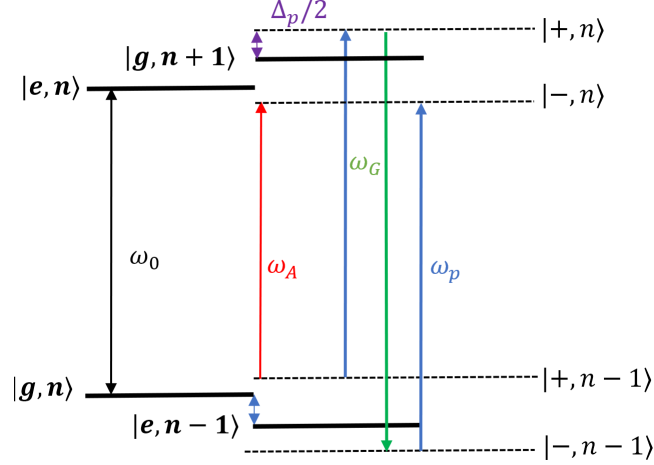


FIG. 5: Atom-photon dressed state picture of the TLS in the case when the pump pulse is off resonance; ω_A corresponds to an absorption feature that appears with non-resonant driving; $\omega_G = 2\omega_{pr} - \omega_A$ is the probe frequency that corresponds to the three-photon scattering amplification side-band.

Figure 5 shows various spectral lines corresponding to features in the absorption spectrum for the slightly detuned case as in Fig. 4. In the atom-photon number dressed state basis, we see that the features correspond to transitions between different dressed states involving absorption/emission of a probe photon with energy $\hbar\omega_{pr}$ and absorption/emission of a number of pump photons with energy $\hbar\omega_p$.

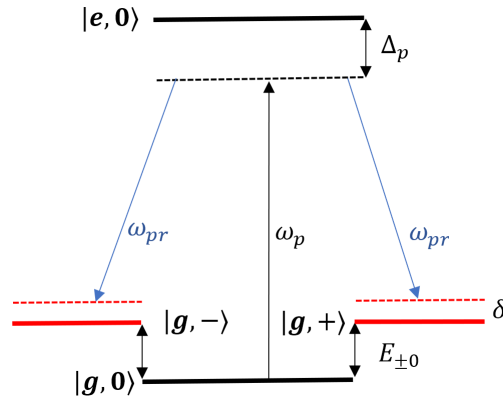


FIG. 6: Raman gain in a detuned system with multiple magnetic sub-levels. $|g, m\rangle$ is the ground state magnetic sub-level m . The pump field (ω_p) and spontaneous decay create a population distribution among the $|g, m\rangle$ states that depends on their Clebsch-Gordan coefficients. The probe laser (ω_{pr}) experiences gain/loss depending on the signs of Δ_p , δ .

C. Raman gain using Zeeman sublevels

For the case of a two-level system with many magnetic sub-levels, a far-detuned pump laser field can induce probe gain through population inversion among the shifted sub-levels. Unlike Mollow gain, Raman gain on magnetic sublevels requires a probe field with polarization orthogonal to the pump field polarization¹⁴. This is due to the necessary two-photon Raman transition between different m number states. The high one-photon detuning creates level shifts of the dressed states corresponding to each magnetic sub-level and introduces a dispersive structure for the absorption spectrum at $\delta = 0$ shown in Fig. 6. This results in gain on one side of the structure and loss on the other, shown in Fig. 7.

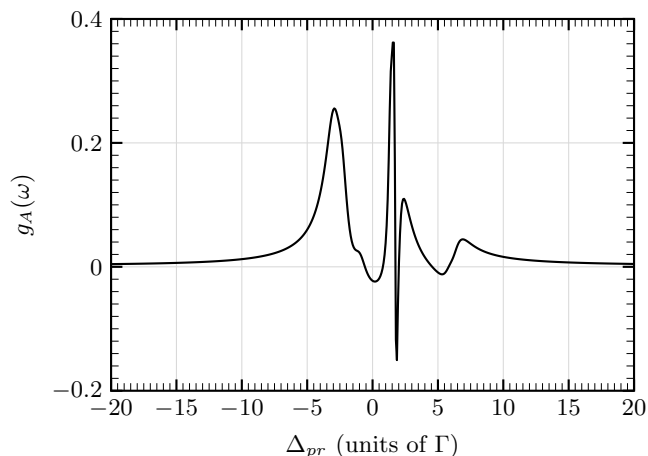


FIG. 7: Absorption spectrum of light with perpendicular polarization for the off-resonantly driven ^{87}Rb system with parameters $\Gamma = 1.0$, $\Omega_p = 4\Gamma$, $\Delta_p = 1.75\Gamma$.

D. Raman gain with coupling fields

Raman gain can be induced by sustaining a population inversion between two different lower energy states, e.g. hyperfine ground states²⁰ through optical pumping, and then producing gain with a stimulated two-photon transition using a coupling field $E_c(t)$ ^{20,38}. The probe polarization in this case depends on the choice of level $|e_2\rangle$, see Fig. 8.

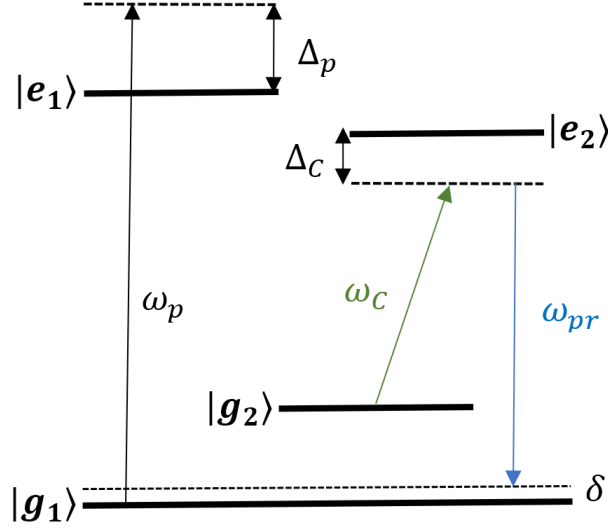


FIG. 8: Raman gain in a system with coupled hyperfine levels g_i . The pump laser (ω_{pr}) optically pumps the system to induce ground state coherence. The coupling laser (ω_C) is introduced to return atoms to the ground states and create gain in the probe (ω_p) due to the Raman transition involving the coupling and probe.

E. Four-wave mixing (FWM) gain

FWM is a phase-sensitive parametric nonlinear optical process that involves the interactions of four fields with a nonlinear medium and transferring energy between the fields³⁹. When considering a degenerate FWM (d-FWM) using counter-propagating pump fields and satisfying a phase matching condition, gain is observed in the backward propagating reflection of the probe field^{20,40}.

F. Inversionless gain in coherently driven multilevel systems

Probe gain in coherently driven multilevel systems without inversion in any meaningful basis has been described as resulting from coherence between dressed states^{31,32}. For the case of the three-level V-system, each of the coherent, linked dressed state contributes to the absorption spectrum with two independent Lorentzians occurring at the dressed states resonances. The presence of gain is suggested to be due to competition between n-photon scattering processes, each of which is responsible for contributing to gain or loss. In V and Λ type systems, two-photon scattering is responsible for inversionless gain, while one-photon

processes cause gain in cascade type systems³².

G. Amplified Spontaneous Emission (ASE)

Spontaneous emission is a quantum process in which an atom in an excited state spontaneously de-excites into a lower energy state by emitting a photon into one of the modes of the quantum mechanical vacuum/reservoir field. It can be semiclassically described as emission process stimulated by vacuum noise, (the zero-point fluctuations of the electric field in the vacuum state)⁴¹. ASE is a result of stimulated emission processes that amplify the spontaneous radiation field propagating in a medium with gain and is often a pervasive phenomenon in lasers and optical amplifiers⁴². We distinguish between ASE and the cooperative phenomena of superfluorescence, the latter process requiring negligible dephasing to form a coherent macroscopic interaction⁵.

The threshold for ASE in a particular gain medium is reached when the contribution from optical gain processes is greater than that of absorption and escape processes, (radiation scattering away from the medium). Unlike lasing involving coherent amplification of the probe pulse, the temporal coherence of ASE in media with multiple scatterers without coherent feedback is often low, due to a large radiation bandwidth. In particular, the second-order coherence $g^{(2)}(\omega, t)$ of ASE demonstrates super-Poissonian statistics consistent with that of thermal light⁴³. However the presence of a coherent feedback loop realizes random lasing and the generation of more coherent light with Poissonian statistics⁴⁴. Coherent feedback loops can be created by manipulating the scattering processes in the gain medium, as multiple scattering can replace the requirement of mirrors for coherent feedback. This leads to the formation of a new threshold for lasing with coherent feedback that depends on the gain medium's scattering properties⁴⁵.

The spatial coherence of ASE can be very high even without a coherent feedback loop. In atomic gas systems, the geometry of the lasing setup (the optically active part of the system), as well as the internal degrees of freedom (atomic populations, coherences and the spectral lineshape⁴⁶), affect spatial coherence and beam divergence. The treatment of spatial coherence becomes more complicated when considering multiple scattering, especially in the strong scattering regime where localization of light can occur⁶.

The starting point for the microscopic treatment of ASE in a continuously driven medium

is the Heisenberg equations of motion for the photon number operator Eq. (9). In general, it is difficult to solve for the photon number operator, especially in the case of large systems. Instead, the operator $\langle E_{I'}^{(\mu)-}(\vec{r}) E_{I'}^{(\mu')+}(\vec{r}) \rangle(t)$ is considered. Before we look at the effects of feedback and multiple scattering, we look into this operator in detail. The contribution of spontaneous emission in $\langle E_{I'}^{(\mu)-}(\vec{r}, t) E_{I'}^{(\mu')+}(\vec{r}, t) \rangle$ is

$$S_s(t) = \sum_{j,\alpha} \sum_{i,\beta;\nu=\pm} \int_0^t dt' \left(\Gamma_{ji}^{(\mu\mu')}(\vec{R}_\alpha, \vec{R}_\beta, t, t') \langle \sigma_{i,I'}^+(\vec{R}_\alpha, t) \sigma_{j,I'}^-(\vec{R}_\beta, t') \rangle \right. \\ \left. + \Gamma_{ij}^{(\mu\mu')}(\vec{R}_\alpha, \vec{R}_\beta, t, t') \langle \sigma_{j,I'}^+(\vec{R}_\beta, t') \sigma_{i,I'}^-(\vec{R}_\alpha, t) \rangle \right), \quad (16)$$

where $\Gamma_{ij}^{(\mu\mu')}(\vec{R}_\alpha, \vec{R}_\beta, t, t')$ is given by

$$\int \int d^3k d^3k' g_{\vec{k};i}^{(\mu)}(\vec{R}_\alpha, t) g_{\vec{k}';j}^{(\mu')*}(\vec{R}_\beta, t'). \quad (17)$$

We distinguish between the single-atom term ($\alpha = \beta$) and the two-atom terms ($\alpha \neq \beta$). The latter contributes to collective emission, the superfluorescence. The stimulated emission term is

$$\mathcal{R}_s(t) = i \sum_{i,\alpha} \int \int d^3k d^3k' \left(g_{\vec{k}';i}^{(\mu')*}(\vec{R}_\alpha) \text{Tr} \left\{ a_{\vec{k},I'}^{(\mu)\dagger}(t) \sigma_{i,I'}^-(\vec{R}_\alpha, t) \rho_{I'}(t_0) \right\} \right. \\ \left. - g_{\vec{k};i}^{(\mu)}(\vec{R}_\alpha) \text{Tr} \left\{ a_{\vec{k},I'}^{(\mu')}(t) \sigma_{i,I'}^+(\vec{R}_\alpha, t) \rho_{I'}(t_0) \right\} \right) \\ - \sum_{ij,\alpha;\nu=\pm} \int_0^t dt' \left(\langle E_{I'}^{(\mu)-}(\vec{r}, t) \left[\vec{d}_l \cdot \vec{E}_{I'}^{(\nu)+}(\vec{R}_\alpha, t') \right] \cdot \mathcal{C}_{i,j}^{(\mu')}(\vec{r}, \vec{R}_\alpha, t, t') \rangle \right. \\ \left. + \langle \left[\vec{d}_l^* \cdot \vec{E}_{I'}^{(\nu)-}(\vec{R}_\alpha, t') \right] E_{I'}^{(\mu')+}(\vec{r}, t) \cdot \mathcal{C}_{i,j}^{(\mu)\dagger}(\vec{r}, \vec{R}_\alpha, t, t') \rangle \right). \quad (18)$$

The first term, the Langevin force, is non-zero only if there are initial correlations at time t_0 . The \vec{d}_l is the unit transition dipole vector for transition l . The term proportional to the single-atom dipole correlation operator reads

$$\mathcal{C}_{i,k}^{\mu'}(\vec{r}, \vec{R}_\alpha, t, t') = \left[\sigma_{i,I'}^-(\vec{R}_\alpha, t), \sigma_{j,I'}^+(\vec{R}_\alpha, t') \right] \times \int d^3k' g_{\vec{k}';i}^{(\mu')*}(\vec{R}_\alpha - \vec{r}) \varepsilon_{\vec{k}}^{(\mu')}. \quad (19)$$

The single-atom dipole-dipole functions are expanded in terms of projection operators onto the populations and coherences to give us the contributions to the spontaneous emission and gain/loss spectra. In the case where we have non-degenerate levels and no driving fields, one transition is coupled to each radiation mode, and single-atom dipole-dipole functions for transition l are equal to sums of σ_l^z and I_l . Coupling multiple transitions to a single mode

introduces lower-state or upper-state coherence. The contribution from each transition is weighted by their Clebsch-Gordan coefficient and the transition frequency.

In the field interaction picture where the atomic propagators are dressed with the driving field, non-zero driving introduces the σ_l^\pm operators in the dipole-dipole functions, thus introducing dependence on the atomic coherences. In this way, the dressed state structure of the degenerate system appears with the presence of new Lorentzians and interference terms in the spectral function. Since the atomic coupling to the vacuum is weak, it is useful to switch to the more physically meaningful basis of the dressed states which are the eigenstates of $U_L(t, t_0)$.

We assume that driving fields are slowly varying, with small losses in the intensities over large timescales. The dressed states, $|\Lambda_k(\vec{R}_\alpha, t)\rangle$, are defined along with their corresponding energies $\lambda_k(t)$ such that

$$\sigma_{j;l'}^+(\vec{R}_\alpha, t) = \sum_{m'm} C_{m'm}^j(\vec{R}_\alpha, t) e^{it(\omega_j + \lambda_{m'} - \lambda_m)} |\Lambda_m(\vec{R}_\alpha, t)\rangle \langle \Lambda_{m'}(\vec{R}_\alpha, t)|. \quad (20)$$

The dipole-dipole function consists of projection operators onto the dressed state populations and coherences. This causes all fast time dependencies to be stored in the exponentials and the density matrix. Due to small coupling strength, and with the assumption that transition frequencies are in the optical regime, the timescale for the evolution of the density matrix is significantly larger than that for the decay of the correlation functions. This justifies the use of the Markov approximation.

H. Paraxial approximation

A pencil-like geometry for the pump laser is assumed such that only a narrow cone of wavevectors Σ_k , for forwards (R) and backwards (L) components, contributes to the ASE modes. The electric field operator for a single mode $\hat{E}^{(\mu)}(\vec{r}, t)$ is therefore expanded as:

$$\hat{E}^{(\mu)}(\vec{r}, t) = \left[E_R^{(\mu)+}(\vec{r}, t) e^{i\vec{k}_0 \cdot \vec{r}} + E_L^{(\mu)+}(\vec{r}, t) e^{-i\vec{k}_0 \cdot \vec{r}} \right] e^{-i\omega_0 t} - \text{H.c.}, \quad (21)$$

where \vec{k}_0 is the forward propagating wavevector along the axis of Σ_k and $E_k^{(\mu)+}(\vec{r}, t)$ is a slowly varying operator. This treatment is similar to the description of ASE for the case of homogeneously broadened three-level atoms in a rod-like geometry⁴⁷. We assume that the atomic density is large enough that the dipole operator is now a continuous function

of position. Furthermore we assume in a small volume V_r with radius r centered at any point \vec{R} , the $\omega_j c^{-1} r \gg 1$, and the dipole correlation function and the atomic density varies trivially. We introduce the volume-averaged dipole in a small vertical slice of the cylindrical medium $S_{j;I'}^+(\vec{R}_i, t) = n(\vec{R}_i) \int_{V_r(\vec{R}_i)} dV' \sigma_{j;I'}^+(\vec{R}', t)$. The interaction terms between pairs of atoms are assumed to contribute negligibly to the dynamics and are ignored. The equation for the density matrix element in the dressed state basis reads

$$\begin{aligned}
\frac{d}{dt} \left\langle \sigma_{\Lambda_a \Lambda_b}(\vec{R}_a, t, t) \right\rangle_{I'} &= \sum_{ml} \Gamma_1^{ab;ml}(\vec{R}_\alpha, t) \left\langle \sigma_{\Lambda_m \Lambda_l}(\vec{R}_a, t, t) \right\rangle_{I'} \\
&\quad - \sum_l \Gamma_2^{ab;l}(\vec{R}_\alpha, t) \left\langle \sigma_{\Lambda_a \Lambda_l}(\vec{R}_a, t, t) \right\rangle_{I'} \\
&\quad - \sum_l \Gamma_3^{ab;l}(\vec{R}_\alpha, t) \left\langle \sigma_{\Lambda_l \Lambda_b}(\vec{R}_a, t, t) \right\rangle_{I'} \\
&\quad + \sum_{\hat{k}_1, \hat{k}_2} I^{(\mu\mu')}(\hat{k}_1, \hat{k}_2, \vec{R}_\alpha, \vec{R}_\alpha, t) \\
&\quad \times \left(\sum_{ml} B_1^{ab;ml}(\mu, \mu', \vec{R}_\alpha, t) \left\langle \sigma_{\Lambda_m \Lambda_l}(\vec{R}_a, t, t) \right\rangle_{I'} \right. \\
&\quad + \sum_{ml} B_2^{ab;l}(\mu, \mu', \vec{R}_\alpha, t) \left\langle \sigma_{\Lambda_a \Lambda_l}(\vec{R}_a, t, t) \right\rangle_{I'} \\
&\quad \left. + \sum_{ml} B_3^{ab;l}(\mu, \mu', \vec{R}_\alpha, t) \left\langle \sigma_{\Lambda_l \Lambda_b}(\vec{R}_a, t, t) \right\rangle_{I'} \right). \tag{22}
\end{aligned}$$

We define the two-point field correlation function as $I^{(\mu\mu')}(\hat{k}_1, \hat{k}_2, \vec{R}_1, \vec{R}_2, t) = \left\langle E_{\hat{k}_1, I'}^{(\mu)-}(\vec{R}_1, t) \vec{E}_{\hat{k}_2, I'}^{(\mu') +}(\vec{R}_2, t') \right\rangle$. The term $\vec{R}_{1,2}$ is the average polarization vector of the \mp field component and $\hat{k}_{1,2} \in \{L, R\}$. We use the paraxial approximation formalism described in Ref. ⁴⁷ to derive the radiative transport equation

$$\begin{aligned}
\left[\frac{\partial}{\partial t} + c \left(\hat{k}_1 \cdot \nabla_{\vec{R}_1} + \hat{k}_2 \cdot \nabla_{\vec{R}_2} \right) \right. \\
\left. - i \frac{c}{2k_0} \nabla_{\perp}^2 \right] I^{(\mu\mu')}(\hat{k}_1, \hat{k}_2, \vec{R}_1, \vec{R}_2, t) &= \sum_{\vec{x}, ij} A_{\mu\mu'}^{ij;ml}(\vec{x}, t) \left\langle S_{\Lambda_m \Lambda_l}(\vec{x}, t, t) \right\rangle_{I'} \\
&\quad + \sum_{\hat{q} \in \{L, R\}} \sum_{\vec{x}, ij} \delta_{\mu\mu'} \left\langle S_{\Lambda_m \Lambda_l}(\vec{x}, t, t) \right\rangle_{I'} \\
&\quad \times \left[K^{ij;ml}(\hat{q} \rightarrow \hat{k}_1, \hat{k}_2, \vec{x}, t) I^{(\mu\mu)}(\hat{q}, \hat{k}_2, \vec{R}_1, \vec{R}_2, t) \right. \\
&\quad \left. + K^{ij;ml}(\hat{k}_1, \hat{q} \rightarrow \hat{k}_2, \vec{x}, t) I^{(\mu\mu)}(\hat{k}_1, \hat{q}, \vec{R}_1, \vec{R}_2, t) \right], \tag{23}
\end{aligned}$$

where ∇_{\perp} is the gradient operator transverse to $\hat{k}_{1,2}$ and $A_{\mu\mu'}^{ij;ml}(\vec{x}, t)$ is given by

$$\begin{aligned}
A_{\mu\mu'}^{ij;ml}(\vec{x}, t) = & \int_{\Sigma_k} \int_{\Sigma_{k'}} d^3k d^3k' g_{\vec{k};i}^{(\mu)*}(\vec{x}) g_{\vec{k}';j}^{(\mu')}(\vec{x}) \\
& \times \sum_{l'} \int_0^{\infty} d\tau \left[C_{l'l}^{i*}(t) C_{ml'}^j(t) e^{-i(\omega_k - \omega_{k'} - \omega_{ij} + \lambda_{l'l} - \lambda_{l'm})t} e^{i(\omega_{k'} - \omega_j + \lambda_{l'm})\tau} \right. \\
& \left. + C_{ml'}^i(t) C_{l'l}^{j*}(t) e^{i(\omega_k - \omega_{k'} - \omega_{ij} - \lambda_{l'l} + \lambda_{l'm})t} e^{-i(\omega_{k'} - \omega_j - \lambda_{l'm})\tau} \right]. \tag{24}
\end{aligned}$$

The spontaneous emission contribution is integrated over the cone in momentum space that contains wave-vectors that remain in the cylindrical medium and contribute to ASE. The remaining wavevectors are considered to have escaped from the medium and do not contribute to the evolution of the paraxial ASE modes. $K^{ij;ml}(\hat{q} \rightarrow \hat{k}_1, \hat{k}_2, \vec{x}, t)$ and $K^{ij;ml}(\hat{k}_1, \hat{q} \rightarrow \hat{k}_2, \vec{x}, t)$ are the scattering probabilities for the mode with wavevector \hat{q} to scatter into the mode with wavevector $\hat{k}_{1,2}$ respectively through virtual transitions between dressed states Λ_m and Λ_l . This corresponds to stimulated emission processes and is derived from Eq. (18) using the dressed state expansion of the atomic operators Eq. (20).

The paraxial approximation equations for the dressed state atomic matrix and the radiative equations for the field correlation effectively model the dynamics of an ASE field in a cold random atomic gas, under the approximation that interatomic scattering plays little to no effect. The gain condition that results in ASE can be derived by calculating all the coefficients that depend on the dressed state configuration and determining the choices of parameters, including the pump field and detuning, that result in the right-hand side of Eq. (23) being greater than zero in the steady state. The choice of parameters can be informed by looking at the gain mechanisms, and the above section on the probe field gain accounts for how dressed state inversions and coherences contribute.

I. Gain analysis

We define the specific intensity $I_{e_i}(\vec{r}, t, \hat{k}, \omega)$ which describes the rate of radiative transfer at point (\vec{r}, t) for the field with polarization e_i and wavevector \vec{k} emitted from a unit area through a unit solid angle. A simplified model for $I_{e_i}(\vec{r}, t, \hat{k}, \omega)$ is given under the assumption of small optical amplification of the spontaneous emission field, steady state atomic dynamics, and no Doppler and collision-caused frequency redistribution and broadening effects.

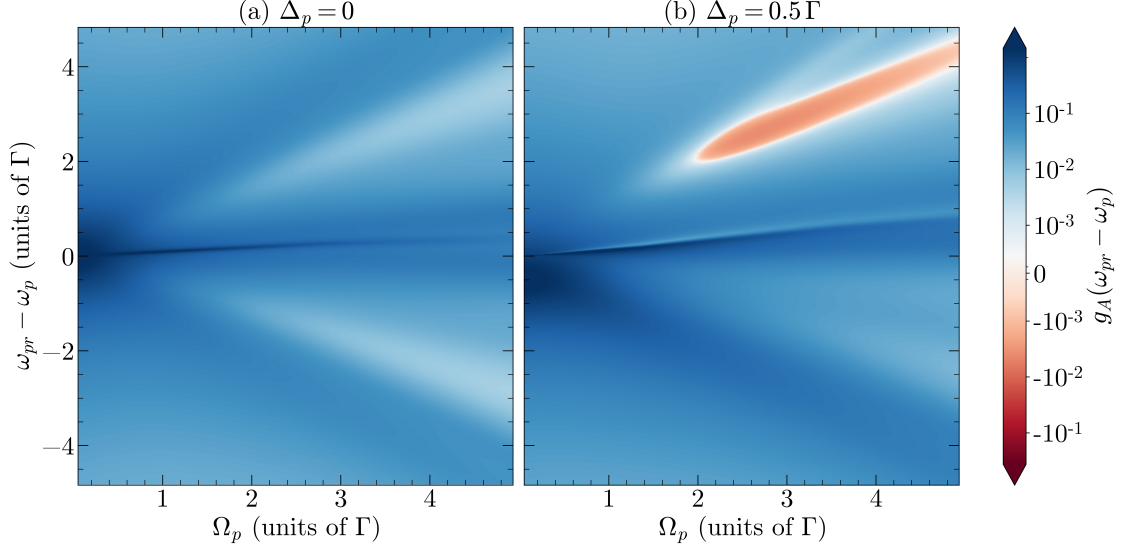


FIG. 9: Graph of absorption value over the entire spectrum of radiation for the orthogonally polarized (to the pump) field (seeded by the probe) versus the pump Rabi frequency. The ^{87}Rb $F_g = 2 \rightarrow F_e = 3$ system is used with parameters $\Gamma = 1.0$, (a) $\Delta_p = 0$ and (b) $\Delta_p = 0.5\Gamma$. The probe field frequency that corresponds to the minimum absorption feature varies with Δ_p and Ω_p . Gain is only observed when the one-photon detuning is non-zero (red area).

For $\frac{\partial I_x(\vec{r}, t, \hat{y}, \omega)}{\partial t} = 0$, the radiative transfer equation has the form¹⁷

$$\frac{\partial I_x(\vec{r}, t, \hat{y}, \omega)}{\partial y} = \eta(\vec{r}, t) - \chi(\vec{r}, t)I_x(\vec{r}, t, \hat{y}, \omega), \quad (25)$$

$\eta(\vec{r}, t)$ and $\chi(\vec{r}, t)$ are the spontaneous emission contribution and the stimulated absorption term. In the homogenous steady-state atomic medium limit with atom density n_A ,

$$\eta(\vec{r}, t) = n_A \frac{\hbar\omega_0}{4\pi} A(\omega_0) g_E(\omega) = n_A \frac{c|\mu_x|^2}{12\pi\epsilon_0} \left(\frac{\omega_0}{c}\right)^4 \int_0^\infty d\tau \langle d_{x,H}^+(\tau) d_x^- \rangle e^{-i\omega\tau}, \quad (26)$$

$$\chi(\vec{r}, t) = n_A \frac{\hbar\omega_0}{4\pi} B(\omega_0) g_A(\omega) = n_A \frac{\hbar\omega_0}{4\pi} \left(\frac{\pi^2}{c\hbar} \left(\frac{\omega_0}{c}\right)^{-3} A(\omega_0)\right) \int_0^\infty d\tau \langle [d_x^-, d_{x,H}^+(\tau)] \rangle e^{-i\omega\tau}, \quad (27)$$

where $g_{A/E}(\omega)$ is the absorption/emission spectral line shape function, and $A(\omega_0)$, $B(\omega_0)$ are the Einstein coefficients for spontaneous emission and stimulated emission respectively⁴⁸.

The solution to Eq. (25), using boundary condition $I_x(0, t, \hat{y}, \omega) = 0$, is given by,

$$I_x(\vec{r}, t, \hat{y}, \omega) = \frac{g_E(\omega)}{g_A(\omega)} \left(\frac{\hbar\omega_0^3}{\pi^2 c^2}\right) (1 - e^{-\chi(\omega)x}). \quad (28)$$

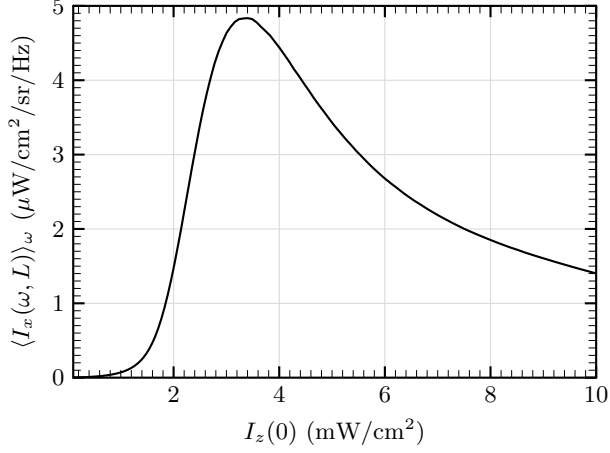


FIG. 10: Graph of averaged specific intensity of the orthogonally polarized radiation copropagating with the pump field versus the pump field intensity. The ^{87}Rb $F_g = 2 \rightarrow F_e = 3$ system⁴⁹ is used with $\Delta_p = 0.5\Gamma$. The cell length is $L = 0.1$ m and the atomic density is $n_A = 1.6 \times 10^{14} \text{ m}^{-3}$.

The absorption spectral response as a function of the Rabi frequency of the pump field is shown in Fig. 9(a) for the resonant ($\Delta_p = 0$) and Fig. 9(b) for the detuned case ($\Delta_p = 0.5\Gamma$). The `Qutip` function library was used to calculate the spectrum using a fast Fourier transform of the two-time correlation function, Eq. (11), in the field interaction picture where the Hamiltonian is time independent. Under the resonance condition, we see that there is no gain for any value of the Rabi frequency. Meanwhile, non-zero detuning provides gain for certain values of the pump field Rabi frequency, as shown by the red area in Fig. 9(b). We define the set of frequencies in this area as the gain island $S_g = \{\omega \mid g_A(\omega) < 0, \Omega_p \leq 5\}$.

The intensity of the generated field averaged over the frequency range within the gain island is shown in Fig. 10 as a function of the pump field intensity for the ^{87}Rb D_2 $F = 2 \rightarrow F = 3$ transition with $n_A = 1.6 \times 10^{14} \text{ m}^{-3}$, $\Delta_p = 0.5\Gamma$ and $x = 0.1$ m. The Rabi frequency corresponding to the maximum gain in the gain island in Fig. 9 (b) is equal to $\Omega_G \approx 2.5\Gamma$. The maximum intensity of the ASE field similarly results for $\Omega_p = \Omega_G$ with the frequency peak at $\omega = \omega_0 + \sqrt{\Omega_G^2 + \Delta_p^2}$.

III. DEGENERATE MIRRORLESS LASING

In this section, we study a prototypical system in which directional emission was predicted and observed to occur at the same frequency and orthogonal polarization as those of the

excitation light.

Consider the eight-level system of the D_2 ($5^2S_{1/2} \rightarrow 5^2P_{3/2}$) line in ^{87}Rb . The $5^2S_{1/2}$ and $5^2P_{3/2}$ states are split into hyperfine structure components with total angular momentum $F_g = 2, 1$ and $F_e = 3, 2, 1, 0$ respectively. We consider the $F_g = 1 \rightarrow F_e = 2$ transition. In the absence of magnetic field, the ground state is three-fold and the excited state is five-fold degenerate.

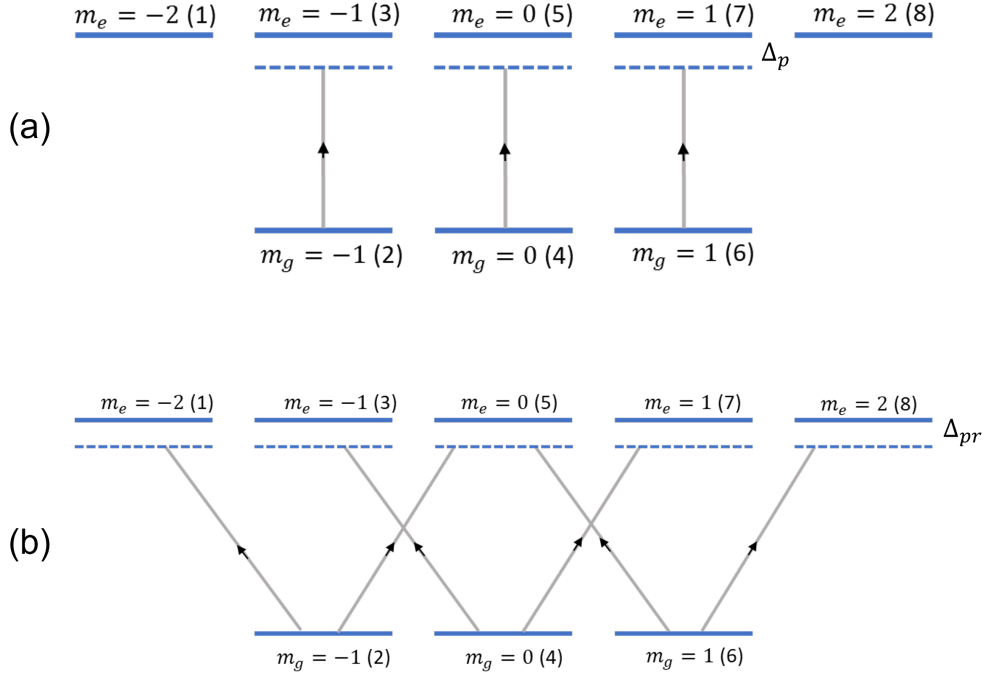


FIG. 11: The degenerate 8-level system interacting with a linearly polarized pump field in z -direction (a) and linearly polarized probe field in the orthogonal direction (b). The numbers given in parenthesis are the numbers corresponding to the levels as they appear in the Hamiltonian.

Pump light linearly polarized in the z -direction induces the transition between magnetic sublevels with the same quantum numbers: $m_g = m_e$. On the other hand, circularly polarized light induces transition between energy level with different magnetic quantum numbers depending on the direction of polarization. This is due to the principle of angular momentum conservation, as the sum of angular momenta of the light and the atom should remain constant. If E_{σ_-} and E_{σ_+} represent the right and left circular polarization components of the light, a superposition of the two components chosen here as the probe gives linearly

polarized field in the \hat{x} direction

$$E_x = \frac{i}{\sqrt{2}}(E_{\sigma_-} + E_{\sigma_+}), \quad (29)$$

where the overall phase factor is chosen for consistency with standard definitions.

A. Population Dynamics

The interaction of the mutually orthogonal linearly polarized pump and probe fields with atoms is depicted in Fig. 11. The pump field polarized along the quantization axis z couples the ground and excited states satisfying the condition $\Delta m = m_e - m_g = 0$, as shown in Fig. 11(a). The orthogonally polarized probe field couples states satisfying $\Delta m = m_e - m_g = \pm 1$, see 11(b).

The field-interaction Hamiltonian is given by:

$$H = \frac{\hbar}{2} \begin{pmatrix} 2\Delta_{pr} & -i\Omega_{21(pr)} & 0 & 0 & 0 & 0 & 0 & 0 & 0 \\ i\Omega_{21(pr)} & 0 & \Omega_{23(p)} & 0 & i\Omega_{25(pr)} & 0 & 0 & 0 & 0 \\ 0 & \Omega_{23(p)} & 2(\Delta_p + \Delta_{pr}) & -i\Omega_{43(pr)} & 0 & 0 & 0 & 0 & 0 \\ 0 & 0 & i\Omega_{43(pr)} & 0 & \Omega_{45(p)} & 0 & i\Omega_{47(pr)} & 0 & 0 \\ 0 & -i\Omega_{25(pr)} & 0 & \Omega_{45(p)} & 2(\Delta_p + \Delta_{pr}) & -i\Omega_{65(pr)} & 0 & 0 & 0 \\ 0 & 0 & 0 & 0 & i\Omega_{65} & 0 & \Omega_{67(p)} & i\Omega_{68(pr)} & 0 \\ 0 & 0 & 0 & -i\Omega_{47(pr)} & 0 & \Omega_{67(p)} & 2(\Delta_p + \Delta_{pr}) & 0 & 0 \\ 0 & 0 & 0 & 0 & 0 & -i\Omega_{68(pr)} & 0 & 0 & 2\Delta_{pr} \end{pmatrix}, \quad (30)$$

where $\Delta_p = \omega_0 - \omega_p$ and $\Delta_{pr} = \omega_0 - \omega_{pr}$ are pump and probe detunings, respectively, and $\Omega_{ij(p,pr)}$ are the Rabi frequencies for transitions between i and j sublevels corresponding to either the pump or the probe field. The Rabi frequencies are given by

$$\Omega_{ij(p,pr)} = -\frac{E_{p,pr}\mu_{ij}}{\hbar} = -\frac{E_{p,pr} \langle F_g m_g | \mathbf{er} | F_e m_e \rangle}{\hbar}, \quad (31)$$

with the interaction strengths characterized by the dipole matrix elements between a ground state $|F_g m_g\rangle$ and an excited state $|F_e m_e\rangle$. To simplify the calculation of Rabi frequencies, the matrix elements are expressed in terms of the 3-j symbol so that the angular momentum

dependence can be factored out:

$$\langle F_g m_g | e\mathbf{r} | F_e m_e \rangle = \langle F_g | e\mathbf{r} | F_e \rangle (-1)^{F_e-1+m_g} \times \sqrt{2F_g+1} \begin{pmatrix} F_e & 1 & F_g \\ m_e & q & -m_g \end{pmatrix}, \quad (32)$$

where $\langle F_g | e\mathbf{r} | F_e \rangle$ is the reduced matrix element, independent of the magnetic quantum numbers and q is the index of \mathbf{r} in the spherical basis. Note that the reduced matrix element will be the same for all transitions. The pump (probe) reduced Rabi frequency Ω_p (Ω_{pr}) can now be defined in terms of the reduced matrix element, such that

$$\Omega_{p,pr} = -\frac{E_{p,pr} \langle F_g | e\mathbf{r} | F_e \rangle}{\hbar}. \quad (33)$$

Any population in the excited state decays to the ground sublevels satisfying the selection rules, $\Delta m = 0, \pm 1$. The decay is characterized by the branching ratio. Considering that the total decay rate of the excited state is Γ , the density matrix equation is given by

$$\frac{d}{dt} \boldsymbol{\rho} = -\frac{i}{\hbar} [\mathbf{H}, \boldsymbol{\rho}] - \frac{\Gamma}{2} \sum_{k=1}^3 (\boldsymbol{\sigma}_k^+ \boldsymbol{\sigma}_k^- \boldsymbol{\rho} + \boldsymbol{\rho} \boldsymbol{\sigma}_k^+ \boldsymbol{\sigma}_k^- - 2\boldsymbol{\sigma}_k^- \boldsymbol{\rho} \boldsymbol{\sigma}_k^+), \quad (34)$$

where $\boldsymbol{\sigma}_k^+$ and $\boldsymbol{\sigma}_k^-$ are the raising and lowering operators for decay channels with $\Delta m = 0$, $\Delta m = -1$ and $\Delta m = +1$ denoted by $k = 1, 2, 3$, respectively.

First, consider that the population is initially distributed equally in the ground sublevels and a cw pump field, linearly polarized in the z -direction, is applied. It induces population transfer with $\Delta m = 0$. Consequently, the states with $|m_e| = 2$ do not obtain any population. The combined process of strong pumping and decay moves populations to sublevels with lower magnetic numbers and eventually brings the system into a steady-state. A useful quantity called saturation parameter, denoted by S , can be defined in terms of the reduced Rabi frequency, spontaneous decay rate and detuning

$$S = \frac{\Omega_p^2}{\frac{\Gamma^2}{4} + \Delta_p^2}. \quad (35)$$

As mentioned earlier, the frequency parameters are expressed in units of Γ and time parameters in the units of $1/\Gamma$. An example of the time evolution of the populations for $S = 36$ is shown in Fig. 12(a). Initially, populations are equally distributed among the three ground degenerate levels. As the system reaches the steady-state, a population inversion between $|m_e| = 0$ and $|m_g| = 1$ levels has been achieved. The one-photon resonance, $\Delta_p = 0$, is favorable for achieving population inversion at lower peak Rabi frequency.

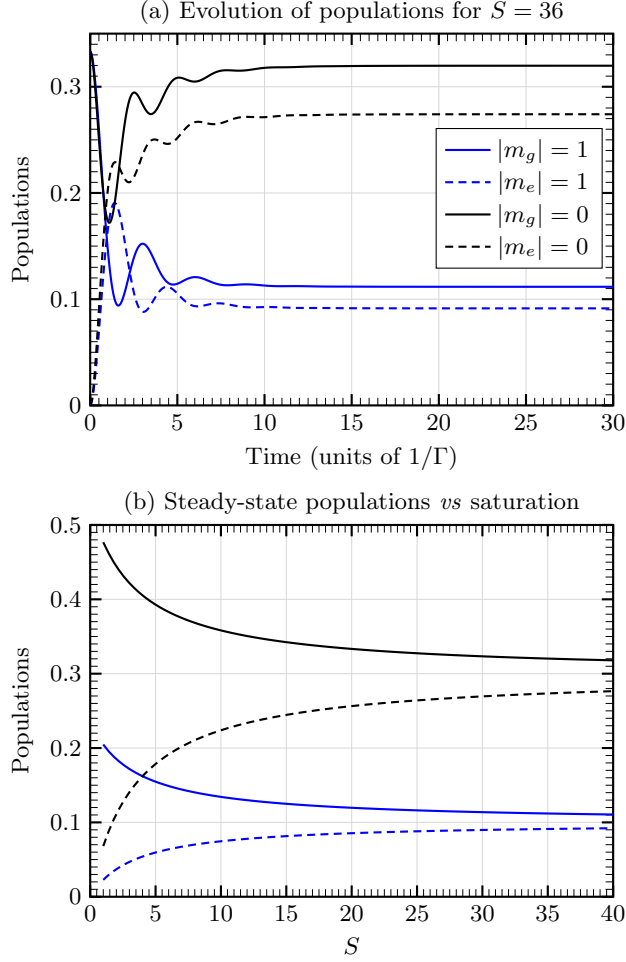


FIG. 12: The evolution of populations for $S = 36$, (a), and the steady-state populations vs saturation parameters (b) in the presence of linearly polarized pump field. Under the combined effect of strong pumping and decay, the populations tend to move towards the hyperfine levels with lower magnetic numbers. While there is no inversion of population between the $m_g = 0$ and $m_e = 0$ levels, there is a population inversion between $|m_g| = 1$ and $m_e = 0$ levels. Since the pump is linearly polarized, the $|m_e| = 2$ levels are not populated at all. Here, $\Delta_p = 0$ and $\Gamma = 1.0$ in both (a) and (b).

In Fig. 12(b), the steady-state populations vs. saturation parameter are depicted. The population inversion is achieved for values of $S > 4.0$, implying a strong pumping is needed for inversion to occur. The pump field is taken here to be in resonance with the transition in both figures 12(a) and 12(b). Taichenachev et al.⁵⁰ have derived equations for the steady state populations in a system with $j_g = j$ to $j_e = j + 1$ energy levels, coupled resonantly to

a pump field. Those steady state equations were derived under the condition that the time derivatives of the density matrix elements are zero. They were used in Ref.²⁵ to calculate populations vs. saturation parameter for the $F_g = 2 \rightarrow F_e = 3$ and $F_g = 3 \rightarrow F_e = 4$ transitions in ^{87}Rb and ^{85}Rb respectively. Figure 12 shows the populations obtained from the exact solution of the Liouville von Neuman equation with relaxation; they are in a good agreement with the ones obtained using steady state equations from⁵⁰ for the $F_g = 1 \rightarrow F_e = 2$ case.

B. The probe field gain

Our objective is to find the conditions for positive gain for probe light polarized orthogonally to the pump field. To achieve this, an equation for amplification (or absorption) of the field is derived from the density matrix equation. Every atom that is de-excited from the upper state emits a photon, which means

$$-\frac{d}{dt}n(\rho^{ex}) = \frac{d}{dt}n_p, \quad (36)$$

where ρ^{ex} stands for the population of the excited state manifold $\rho^{ex} = \sum_{i=1,3,5,7,8} \rho_{ii}$; n and n_p are the atom and photon densities, respectively. Only the photons that are spontaneously emitted within the solid angle Φ will contribute to the intensity in both forward and backward directions. Considering this, the equation for the photon density is written to account for photons emitted due to stimulated and spontaneous emissions separately

$$n_p = n_p^{st} + \frac{\Phi}{4\pi} n_p^{sp}. \quad (37)$$

The light intensity is related to the photons density by $I = n_p c \hbar \omega$ where c is the speed of light and $\hbar \omega$ is the energy of a photon. In Eq.(34), one can identify that the first term is related to stimulated photons generation while the second term to spontaneous emissions. Considering this fact and making use of equality $dz = cdt$, the coupled equations for the propagation of the pump and the probe fields are written as

$$\begin{aligned} \frac{d}{dy} I_z &= -\alpha_z I_z + \frac{\Phi}{4\pi} n \hbar \omega \Gamma_z, \\ \frac{d}{dy} I_x &= -\alpha_x I_x + \frac{\Phi}{4\pi} n \hbar \omega \Gamma_x, \end{aligned} \quad (38)$$

where

$$\begin{aligned}
\alpha_z &= -\frac{n\omega}{2c\epsilon_0 E_{z0}} \sum_{i=1,3,5,7,8} i[\boldsymbol{\mu}_z, \boldsymbol{\rho}]_{ii}, \\
\alpha_x &= -\frac{n\omega}{2c\epsilon_0 E_{x0}} \sum_{i=1,3,5,7,8} i[\boldsymbol{\mu}_x, \boldsymbol{\rho}]_{ii}, \\
\Gamma_z &= \sum_{i=1,3,5,7,8} \frac{\Gamma}{2} (\boldsymbol{\sigma}_1^+ \boldsymbol{\sigma}_1^- \boldsymbol{\rho} + \boldsymbol{\rho} \boldsymbol{\sigma}_1^+ \boldsymbol{\sigma}_1^- - 2\boldsymbol{\sigma}_1^- \boldsymbol{\rho} \boldsymbol{\sigma}_1^+)_{ii}, \\
\Gamma_x &= \sum_{i=1,3,5,7,8} \sum_{k=2,3} \frac{\Gamma}{2} (\boldsymbol{\sigma}_k^+ \boldsymbol{\sigma}_k^- \boldsymbol{\rho} + \boldsymbol{\rho} \boldsymbol{\sigma}_k^+ \boldsymbol{\sigma}_k^- - 2\boldsymbol{\sigma}_k^- \boldsymbol{\rho} \boldsymbol{\sigma}_k^+)_{ii}.
\end{aligned} \tag{39}$$

Here, $\boldsymbol{\mu}_z$ and $\boldsymbol{\mu}_x$ are the matrices with dipole elements corresponding to the transitions of pump and probe fields respectively.

$$\begin{aligned}
\boldsymbol{\mu}_z &= \mu_{23} |2\rangle\langle 3| + \mu_{45} |4\rangle\langle 5| + \mu_{67} |6\rangle\langle 7| + \text{H.c.}, \\
\boldsymbol{\mu}_x &= i \left(\mu_{21} |2\rangle\langle 1| + \mu_{25} |2\rangle\langle 5| + \mu_{43} |4\rangle\langle 3| + \mu_{47} |4\rangle\langle 7| + \mu_{65} |6\rangle\langle 5| + \mu_{68} |6\rangle\langle 8| \right) + \text{H.c.}
\end{aligned} \tag{40}$$

The spontaneous decay factors Γ_z and Γ_x are given by

$$\begin{aligned}
\Gamma_z &= \Gamma \left(b_{32} \rho_{33} + b_{54} \rho_{55} + b_{76} \rho_{77} \right), \\
\Gamma_x &= \Gamma \left(b_{12} \rho_{11} + b_{34} \rho_{33} + (b_{52} + b_{56}) \rho_{55} + b_{74} \rho_{77} + b_{86} \rho_{88} \right),
\end{aligned} \tag{41}$$

where b_{ij} are the branching ratios corresponding to the transitions between i and j states. They read

$$\begin{aligned}
b_{32} &= b_{76} = 1/2, \quad b_{54} = 2/3, \\
b_{12} &= b_{86} = 1, \\
b_{34} &= b_{74} = 1/2, \\
b_{52} &= b_{56} = 1/6.
\end{aligned} \tag{42}$$

The second term of Eq. (38) gives the contribution to the change in intensity due to spontaneous emission of photons of energy $\hbar\omega$ by n atoms per unit volume being in the excited state and decaying to respective ground sub-states connected by z -polarized or x -polarized light. Since the spontaneous decay can be assumed to be isotropic, the factor $\Phi/4\pi$ accounts for the fraction of spontaneously emitted photons into solid angle Φ . The solutions of Eqs. (38) are

$$\begin{aligned}
I_z(y) &= I_{z0} e^{-\alpha_z y} - \frac{\Phi}{4\pi} n \hbar \omega \Gamma_z \left(\frac{e^{-\alpha_z y} - 1}{\alpha_z} \right), \\
I_x(y) &= I_{x0} e^{-\alpha_x y} - \frac{\Phi}{4\pi} n \hbar \omega \Gamma_x \left(\frac{e^{-\alpha_x y} - 1}{\alpha_x} \right),
\end{aligned} \tag{43}$$

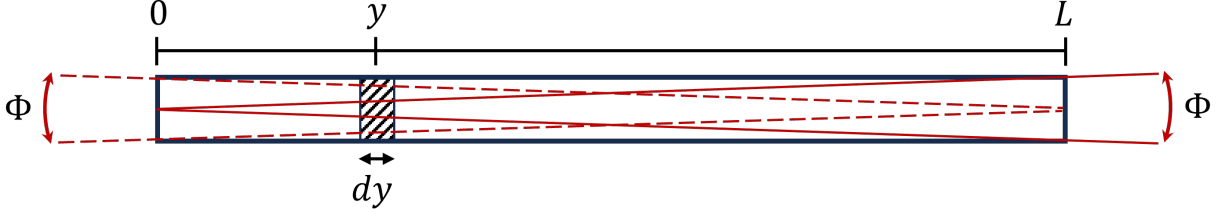


FIG. 13: The geometry of the elongated medium responsible for amplified spontaneous emission whose emission solid angle at both ends of the medium is denoted as Φ .

where $I_{z_0} = I_z(0)$ and $I_{x_0} = I_x(0)$. In the absence of contribution from spontaneous emission, the amplification (or absorption) of the probe field is determined by the absorption coefficient α_x . To analyze this coefficient, it is useful to take the partial trace of the commutator

$$\sum_{i=1,3,5,7,8} i[\boldsymbol{\mu}_x, \boldsymbol{\rho}]_{ii} = 2 \left(\mu_{21} \text{Re}[\rho_{12}] + \mu_{25} \text{Re}[\rho_{25}] + \mu_{43} \text{Re}[\rho_{34}] \right. \\ \left. + \mu_{47} \text{Re}[\rho_{47}] + \mu_{65} \text{Re}[\rho_{56}] + \mu_{68} \text{Re}[\rho_{68}] \right). \quad (44)$$

Because of the symmetry in the system, $\rho_{21} = \rho_{68}$, $\rho_{25} = \rho_{65}$ and $\rho_{43} = \rho_{47}$; the previous equation can hence be reduced to

$$\sum_{i=1,3,5,7,8} i[\boldsymbol{\mu}_x, \boldsymbol{\rho}]_{ii} = 4 \left(\mu_{21} \text{Re}[\rho_{12}] + \mu_{43} \text{Re}[\rho_{34}] + \mu_{65} \text{Re}[\rho_{56}] \right). \quad (45)$$

The sign of the absorption coefficient α_x is opposite to the sign of the quantity in Eq. (45). For the probe field to be amplified, α_x needs to be negative. In Fig. 14, the real and imaginary parts of three relevant coherences ρ_{12} , ρ_{34} and ρ_{56} are plotted for $\Omega_p = 3.0\Gamma$ assuming a negligible probe intensity. Figures 14(a) and 14(b) correspond to the resonant case ($\Delta_p = 0$), and 14(c) and 14(d) correspond to the detuned case $\Delta_p = 0.1\Gamma$. The sum of the real parts of coherences is negative in both cases, leading to the coefficient α_x being positive. The positive value of the real part of coherence ρ_{56} between inverted magnetic sublevels reduces the overall negative value of the sum, thus reducing the degree of absorption. The present case implies that there is no gain in the medium. Note that all imaginary parts are zero in the resonant case. In the detuned case, imaginary parts have non-zero values. However, they do not contribute to the absorption coefficient but to a change in phase of the electric field.

To analyze how detuning impacts the absorption coefficient α_x , it is useful to define a quantity called frequency offset given by $\delta = \omega_{pr} - \omega_p = \Delta_p - \Delta_{pr}$. The absorption

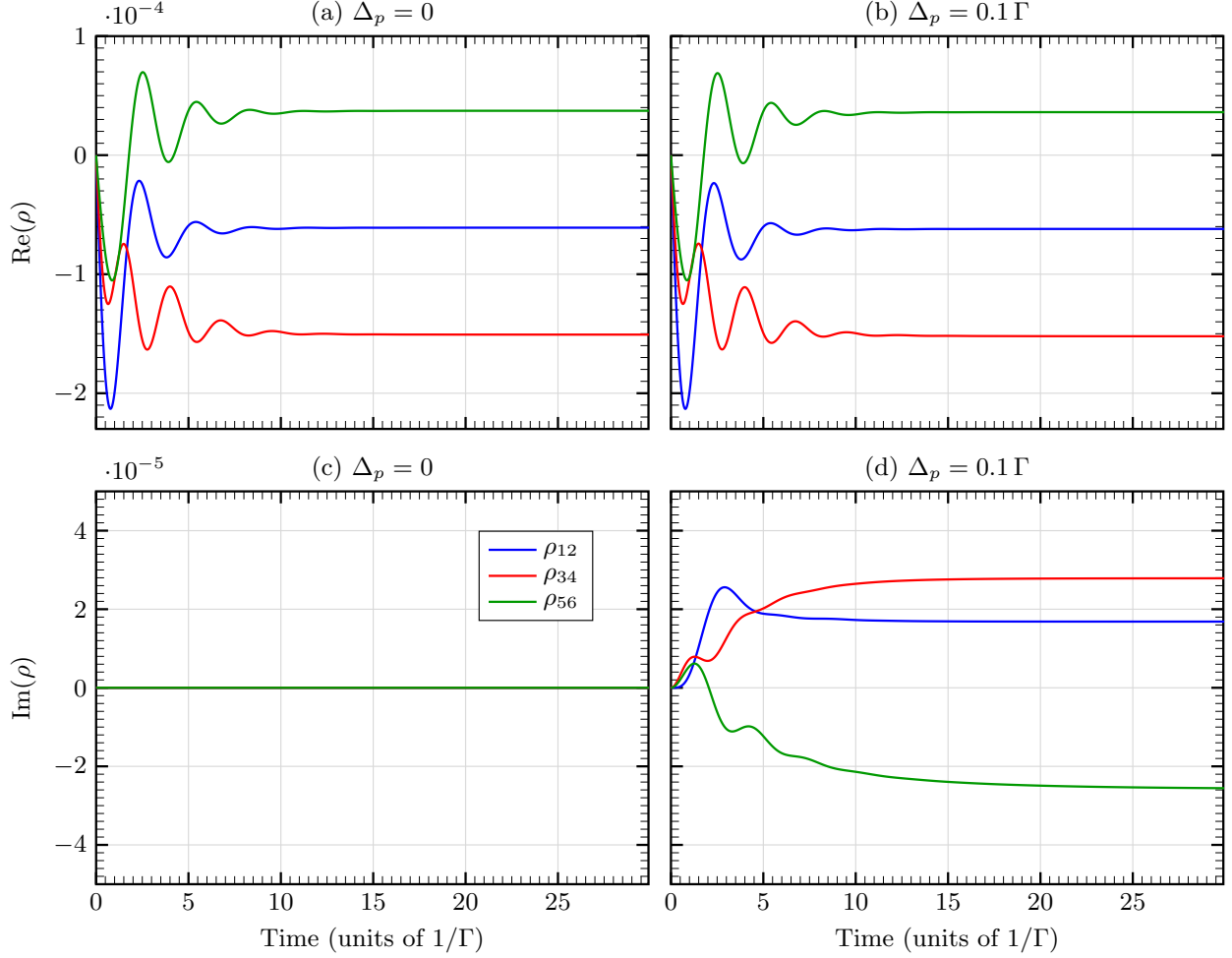


FIG. 14: Coherence between states connected by the probe field. In (a) and (c), $\Delta_p = 0$, and in (b) and (d), $\Delta_p = 0.1\Gamma$. When the pump field is in resonance, imaginary parts of all the coherences are zero. In the presence of detuning, non-zero imaginary parts contribute to a phase change of the field.

coefficient for the degenerate system of $F_g = 1 \rightarrow F_e = 2$, considering a very weak probe field $\Omega_{pr} = 10^{-3}\Omega_p$, is plotted as a function of δ in Fig. 15(a). Here, the pump field frequency is in resonance with the atomic transition frequency, $\Delta_p = 0$. The absorption coefficient is always positive in this case indicating the absence of gain. The peak absorption occurs at the frequency of the probe field in the resonance with the atomic frequency, $\Delta_{pr} = 0$.

To find the output intensity of the generated field having linear polarization orthogonal to polarization of the incident pump field we solve Eq. (38). Once the system is pumped to a steady state, spontaneous photons generate light, which further gets amplified or absorbed

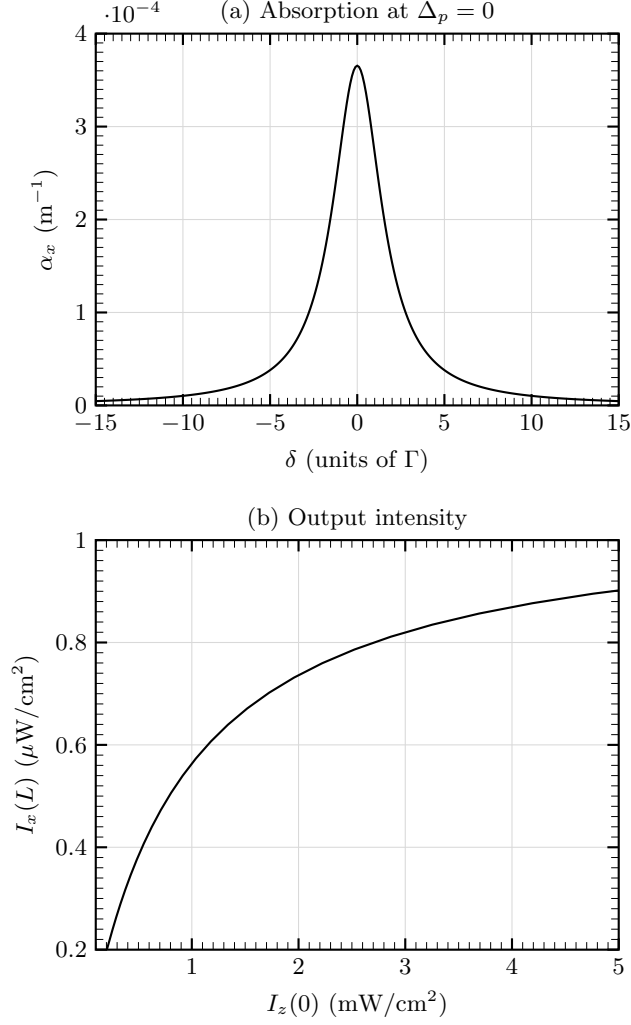


FIG. 15: In (a), the probe field absorption in the case of resonance $\Delta_p = 0$ is plotted as a function of the detuning δ for different pump detunings considering a very weak probe field, $\Omega_{pr} = 10^{-3}\Omega_p$, $\Omega_p = 0.5\Gamma$ for $F_g = 1 \rightarrow F_e = 2$ system. In (b), the output intensity of the field linearly polarized in the x direction as a function of the pump field linearly polarized in the z -direction. The cell length is $L = 0.1$ m and the atomic density is $n_A = 1.16 \times 10^{16} \text{ m}^{-3}$ ²².

depending on the contribution from the first term in Eq. (38). The output field intensity for varying values of the pump field intensity is shown in Fig. 15(b). The output intensity initially varies linearly and followed by saturation at higher intensities of the pump field. The generated field intensity is built from two contributions: one coming from the directional, stimulated coherent process due to induced polarization [first term in Eq. (38)] and the second coming from the amplification of isotropic spontaneous emission [second

term in Eq. (38)]. Population inversion present in the steady atomic state contributes to the stimulated emission/absorption mechanism; yet is not enough to overcome overall losses (absorption from non-inverted states) and hence does not lead to gain but only to a reduced absorption. However, one should expect the output measurement of the generated field having polarization perpendicular to the pump field to be nonzero owing to the isotropic emission of spontaneously emitted photons. The intensity of this field depends on the Rabi frequency and the pump field detuning. As an example for experimental realization, given the decay rate is equal to $\Gamma = 2\pi \times 5.6$ MHz ($^{87}\text{Rb } F = 2 \rightarrow F = 3$), we propose using the Rabi frequency equal to $\Omega_p = 0.4\Gamma$, and the one-photon detuning equal to $\Delta_p = 0.5\Gamma$.

IV. EXPERIMENTAL SITUATION

The idea of degenerate mirrorless lasing was born at the Institute for Physical Research, in Ashtarak, Armenia^{23,25} and evolved into a fruitful collaboration with the University of Mainz a few years later.

The principle idea, as discussed above, is that optical pumping redistributes the population among the ground-state Zeeman sublevels. At sufficiently high light powers of a linearly-polarized radiation, the population is partially transferred to the excited state, which, in the case of an $F \rightarrow F+1$ transition may result in population inversions between certain sublevels of the ground and excited states. Due to the pencil-shaped geometry of the light-atom interaction volume, this inversion may, under right circumstances, result in directional emission from the sample. In the case of degenerate mirrorless lasing, amplified spontaneous emission is produced along or opposite to the pump-beam direction, with polarization orthogonal to that of the pump.

Forward degenerate mirrorless lasing was detected both in Ashtarak and Mainz, showing a typical threshold dependence of the outgoing beam on the incoming beam intensity. The transitions for which we expected and observed the lasing are $F_e > F_g$ cycling transitions in the D_2 line of rubidium, specifically, $^{85}\text{Rb } F_g = 3 \rightarrow F_e = 4$ and $^{87}\text{Rb } F_g = 2 \rightarrow F_e = 3$. The intensity of the emission polarized orthogonally with respect to the incident light was studied as a function of the pump intensity and magnetic field applied along the direction of the pump-light polarization. Up to 1% conversion efficiency was observed at zero-magnetic field, which approached to zero with the applied magnetic field. The width of this feature

was about 15 – 100 mG (FWHM) depending on the pump intensity.

These findings²² are a strong indication of amplified emission in the forward direction, also known as forward mirrorless lasing. In parallel, we detected degenerate four-wave mixing (FWM), which makes the signal more complicated.

While forward mirrorless lasing is an interesting phenomenon, backward mirrorless lasing is of greater interest, since it can be used for remote-detection magnetometry, for example with laser guide stars⁵¹. Indeed, high directivity of the backward beam will significantly facilitate recording of the return flux, which will make the distant remote sensing much easier.

From the theoretical analysis presented in previous sections one can expect that the mirrorless lasing should also take place along the pump beam in the backward direction.

It would seem that mirrorless lasing in the backward direction should be detected even more easily than in the forward direction, since there is no strong background of pump radiation, and also no contribution from the accompanying FWM. However, preliminary experiments have revealed complexities that require further reflection and clarification.

It was possible to record a non-diverging backward emission in Ashtarak with much lower conversion efficiency (almost three orders of magnitude less than for the forward one) at specific experimental conditions. The recorded radiation had an intensity threshold and was sensitive to the applied magnetic field, similar to the forward case, but exhibited sharp sub-Doppler features, which were not observed in the forward lasing. However, this result could not be reproduced in Mainz, even with the same vapor cell and the same experimentalists.

These preliminary studies were useful in identifying the factors important for realization of the backward mirrorless lasing. Among these factors are: (i) careful avoiding of residual birefringence of the vapor cell windows; (ii) proper cancellation and control of the magnetic field; (iii) presence (or absence) of a weak seeding radiation; (iv) broad spectral linewidth of the pump laser.

The much lower conversion efficiency, as well as the narrow spectral features of the backward radiation, should be associated with the competition between the emission and absorption in opposite directions by atoms with different velocities for different pump detunings from Doppler-overlapped atomic transitions.

Further theoretical analysis and experimental studies are needed for complete understanding, as well as unambiguous and reproducible demonstration of backward degenerate

mirrorless lasing.

V. CONCLUSIONS AND OUTLOOK

Degenerate mirrorless lasing is a beautiful phenomenon that has been realized experimentally in the forward direction. However, in the case of backward directed emission, more experimental work needs to be done. At the same time, theoretical guidance is needed to guide and interpret the experimental work.

In this manuscript, we have reviewed the current status of the mirrorless lasing and presented the work-in-progress developments in the general theoretical analysis, hopefully, on the way to a comprehensive solution of the problem.

CONFLICTS OF INTEREST

The authors declare no conflicts of interest.

FUNDING

We recognize the contribution of the tragically deceased Hrayr Azizbekyan. S.M., J.Ch., and A.R. acknowledge support from the Office of Naval Research under awards N00014-20-1-2086 and N00014-22-1-2374. S.M. acknowledges the Helmholtz Institute Mainz Visitor Program and the Alexander von Humboldt Foundation. J.Ch. was also partially supported by DEVCOM Army Research Laboratory under Cooperative Agreement Number W911NF2320076. D.B. was partially supported by DEVCOM Army Research Laboratory under Cooperative Agreement Number W911NF2120180.

Appendix A: Spontaneous emission modes

We use the formalism from²⁹:

We define the field operator:

$$E_H^{(\mu)+}(\vec{r}, t) = \frac{i}{(2\pi)^3} \int d^3k a_{\vec{k},H}^{(\mu)}(t) \sqrt{\frac{\hbar\omega_k}{2\epsilon_0}} e^{i\vec{k}\cdot\vec{r}} \varepsilon_{\vec{k}}^{(\mu)}, \quad (\text{A1})$$

and use the Heisenberg equations of $a_{\vec{k}}^{(\mu)}(t)$:

$$\dot{a}_{\vec{k},H}^{(\mu)}(t) = -i\omega_k a_{\vec{k},H}^{(\mu)}(t) - i \sum_{\alpha,j} g_{\vec{k},j}^{(\mu)*}(\vec{R}_\alpha) \sigma_{j,H}^+(\vec{R}_\alpha, t), \quad (\text{A2})$$

to get the following equation for the Heisenberg operator:

$$\begin{aligned} \square^2 E_H^{(\mu)+}(\vec{r}, t) &= \frac{1}{(2\pi)^{3/2}c} \sum_{\alpha,j} \int d^3k \sqrt{\frac{\hbar\omega_k}{2\epsilon_0}} g_{\vec{k},j}^{(\mu)*}(\vec{R}_\alpha) \varepsilon_{\vec{k}}^{(\mu)} \\ &\times (\omega_k - \omega_j) \sigma_{j,H}^+ \left(\vec{R}_\alpha, t - \frac{|\vec{r} - \vec{r}'|}{c} \right) e^{i\vec{k}\cdot\vec{r}}. \end{aligned} \quad (\text{A3})$$

\square^2 is the D'Alembertian. The right hand side is the total current density, summing over all atomic contributions. We use the Green's function for the D'Alembertian to get the integral:

$$E_{j,H}^{(\mu)+}(\vec{r}, t) = \frac{1}{c} \int d^3r' \frac{J_j^+ \left(\vec{r}', t - \frac{|\vec{r} - \vec{r}'|}{c} \right)}{|\vec{r} - \vec{r}'|}, \quad (\text{A4})$$

and obtain the general solution:

$$\begin{aligned} E_{j,H}^{(\mu)+}(\vec{r}, t) &= \sqrt{\frac{\hbar}{2c^2\epsilon_0(2\pi)^3}} \sum_{\alpha,j} \int d^3r' \int dk d\Omega_k \\ &\times g_{\vec{k},j}^{(\mu)*}(\vec{R}_\alpha) k^3 (\omega_k - \omega_j) \frac{\hat{k} \times (\hat{k} \times \hat{d}_j)}{|\vec{r} - \vec{r}'|} \\ &\times \sigma_{j,H}^+ \left(\vec{R}_\alpha, t - \frac{|\vec{r} - \vec{r}'|}{c} \right) e^{i\vec{k}\cdot\vec{r}}. \end{aligned} \quad (\text{A5})$$

In the far-field limit, the solution simplifies to:

$$\begin{aligned} E_{j,H}^{(\mu)+}(\vec{r}, t) &\propto \sum_{\alpha,j} \frac{\omega_j^2}{c^2} \frac{(\hat{r}_\alpha \cdot \hat{d}_j) \hat{r}_\alpha - \hat{d}_j}{r_\alpha} \\ &\times \sigma_{j,H}^+ \left(\vec{R}_\alpha, t - \frac{r}{c} \right) e^{-i\omega_j(\hat{r}\cdot\hat{r}_j)}. \end{aligned} \quad (\text{A6})$$

where $\vec{r}_\alpha = \vec{r} - \vec{R}_\alpha$.

In the far field, each atom acts as a dipole antenna. In the case where we have many atoms and they're all stationary, a very complicated spatially constant interference pattern emerges. However if the atom has a statistical velocity distribution and the number density is high enough for collisions to be significant, the atomic medium behaves as a chaotic light source.

Appendix B: Paraxial approximation

The volume-averaged dipole operator $S_{j,l}^+(\vec{R}_i, t) = n(\vec{R}_i) \int_{V_r(\vec{R}_i)} dV' \sigma_{j,l}^+(\vec{R}', t)$ is introduced. The volume $V_r(\vec{R}_i)$, center at \vec{R}_i with radius r is chosen as our sampling region where the atomic density matrix and the radiation fields vary trivially in $V_r(\vec{R}_i)$. We use it to simplify the below quantity:

$$\begin{aligned} & \int_{V_r(\vec{R}_i)} dV' \mathcal{C}_{j,l}^{(\mu')}(\vec{r}, \vec{R}', t, t') e^{i(\vec{q}-\vec{k}') \cdot \vec{R}} \\ &= \mathcal{C}_{j,l}^{(\mu')}(\vec{r}, \vec{R}_i, t, t') \int_{V_r(\vec{R}_i)} dV' e^{i(\vec{q}-\vec{k}') \cdot \vec{R}}. \end{aligned} \quad (\text{B1})$$

In the limit of high atomic number density, the condition $\vec{q} = \vec{k}'$ is enforced as other contributions average to 0 as only contributions where the wavevectors are approximately the same survive phase averaging over the volume. With the paraxial approximation, the dot product $\varepsilon_{\vec{k}}^{(\mu)} \cdot \varepsilon_{\vec{k}'}^{(\mu')} \approx \delta_{(\mu\mu')}$. We assume the averaged dipole moment vector $\vec{D}_l(\vec{R}_i) = \int_{V_r(\vec{R}_i)} dV' \vec{d}_l(\vec{R}')$ averages out all fluctuations such that the z-dipole moment, $\vec{D}_z(\vec{R}_i)$, is oriented along the pump polarization axis. Ignoring the Langevin terms, Eq. (18) simplifies to:

$$\begin{aligned} & \mathcal{R}_s(t) \\ &= -\delta_{(\mu\mu')} \sum_{j,l,\alpha;\nu=\pm} \int_0^t dt' \\ & \left(\left\langle (E_{I'}^{(\mu)-}(\vec{r}, t) \vec{E}_{I'}^{(\mu)+}(\vec{r}, t')) (\vec{d}_l \cdot \varepsilon_{\vec{x}}^{(\nu)}) \mathcal{D}_{j,l}(\vec{R}_i, t, t') \right\rangle \right. \\ & \left. + \left\langle \vec{E}_{I'}^{(\mu)-}(\vec{r}, t') E_{I'}^{(\mu)+}(\vec{r}, t) (\vec{d}_l^* \cdot \varepsilon_{\vec{x}}^{(\nu)*}) \mathcal{D}_{j,l}^\dagger(\vec{R}_i, t, t') \right\rangle \right), \end{aligned} \quad (\text{B2})$$

where $\mathcal{D}_{j,l}(\vec{R}_i, t, t')$ is the dipole correlation function Eq. (19).

The expectation of single atom dipole products $\langle \sigma_{i,I'}^+(\vec{R}_i, t) \sigma_{m,I'}^-(\vec{R}_i, t') \rangle$ is expanded in the dressed state basis in terms of operators, defined in the picture I' , $\sigma_{\Lambda_r \Lambda_{r'}}(\vec{R}_i, t, t') = |\Lambda_r(\vec{R}_i, t)\rangle \langle \Lambda_{r'}(\vec{R}_i, t')|$:

$$\begin{aligned} & \sigma_{i,I'}^+(\vec{R}_\alpha, t) \sigma_{j,I'}^-(\vec{R}_\alpha, t') \\ &= -i\hbar \sum_{i,l,l'} \sum_{j,m} C_{ll'}^i(\vec{R}_\alpha, t) C_{mm'}^{j*}(\vec{R}_\alpha, t') e^{it(\omega_i - \omega_j + \lambda_l - \lambda_m)} \\ & \times \sigma_{\Lambda_l \Lambda_m}(\vec{R}_\alpha, t, t') e^{i(\omega_j + \lambda_m - \lambda_{l'}) (t - t')}. \end{aligned} \quad (\text{B3})$$

Assuming the weak coupling approximation, the Markov approximation along with the slow change of $\sigma_{\Lambda_l \Lambda_m}(\vec{R}_\alpha, t, t')$, the coefficients $C_{mm'}(t')$ and the operators are dependent only on time t . The time evolution of the expectation of these operators is given below (The contribution of the stimulated emission and pair-atom terms are ignored):

$$\begin{aligned} & \frac{d}{dt} \langle \sigma_{\Lambda_a \Lambda_b}(\vec{R}_\alpha, t, t) \rangle \\ &= -\frac{i}{\hbar} \int \int d^3k d^3k' g_{\vec{k},i}^{(\mu)}(\vec{R}_\alpha) g_{\vec{k}',j}^{(\mu)*}(\vec{R}_\alpha) \\ & \times \sum_{lm} C_{la}^i(\vec{R}_\alpha, t) C_{am}^{j*}(\vec{R}_\alpha, t) e^{it(\omega_i + \lambda_l - \omega_k)} \\ & \times \int_{t_0}^t dt' \langle \sigma_{\Lambda_a \Lambda_m}(\vec{R}_\alpha, t, t') \rangle e^{-it'(\omega_j + \lambda_m - \omega_{k'})}. \end{aligned} \quad (\text{B4})$$

We now use the Markov approximation. From the standard methods of solving for the spectral line shapes by solving the above equations for all dipole operators in Laplace space, we can determine the power broadened spectral line shapes, $f_{\Lambda_a \Lambda_m}(\omega', t)$, corresponding to $\langle \sigma_{\Lambda_a \Lambda_m}(\vec{R}_\alpha, t, t) \rangle$ and the decay rate $\Gamma_{\Lambda_a \Lambda_m}(t)$. The spontaneous decay rates for the atomic density matrices in the dressed state basis are given below:

$$\begin{aligned} \Gamma_1^{ab;ml}(t) &= \int_0^\infty d\tau \int d^3k \sum_{ij} \left(C_{bl}^{i*}(t) C_{ma}^j(t) g_{\vec{k},i}^{(\mu)*} g_{\vec{k},j}^{(\mu)} \right. \\ & e^{-i(\omega_{ij} + \lambda_{bl} + \lambda_{am})t} e^{i(\omega_k - \omega_j - \lambda_{am})\tau} \\ & \left. + C_{ma}^i(t) C_{bl}^{j*}(t) g_{\vec{k},i}^{(\mu)} g_{\vec{k},j}^{(\mu)*} e^{i(\omega_{ij} + \lambda_{bl} + \lambda_{am})t} e^{-i(\omega_k - \omega_j - \lambda_{bl})\tau} \right), \end{aligned} \quad (\text{B5})$$

$$\Gamma_2^{ab;l}(t) = \int_0^\infty d\tau \int d^3k \sum_{ijl'} \left(C_{l'l}^{i*}(t) C_{l'b}^j(t) g_{\vec{k},i}^{(\mu)*} g_{\vec{k},j}^{(\mu)} \right. \\ \left. e^{-i(\omega_{ij} + \lambda_{l'l} + \lambda_{b'l'})t} e^{i(\omega_k - \omega_j - \lambda_{b'l'})\tau} \right), \quad (\text{B6})$$

$$\Gamma_3^{ab;l}(t) = \int_0^\infty d\tau \int d^3k d^3k' \sum_{ijl'} \left(C_{l'l'}^i(t) C_{l'a}^{j*}(t) g_{\vec{k},i}^{(\mu)} g_{\vec{k},j}^{(\mu)*} \right. \\ \left. e^{i(\omega_{ij} + \lambda_{l'a} + \lambda_{l'l})t} e^{-i(\omega_k - \omega_j - \lambda_{l'a})\tau} \right). \quad (\text{B7})$$

REFERENCES

1. J. Hecht, *Optical Engineering* **49**, 091002 (2010), URL <https://doi.org/10.1117/1.3483597>.
2. A. E. Siegman, *Lasers* (University Science Books, 1986).
3. M. O. Scully, S. Y. Zhu, and H. Fearn, *Zeitschrift für Physik D Atoms, Molecules and Clusters* **22**, 471 (1992), ISSN 1431-5866, URL <https://doi.org/10.1007/BF01426089>.
4. T. Dudok and Y. Nastishin, *Ukrainian Journal of Physical Optics* **14**, 146 (2013).
5. M. S. Malcuit, J. J. Maki, D. J. Simkin, and R. W. Boyd, *Phys. Rev. Lett.* **59**, 1189 (1987), URL <https://link.aps.org/doi/10.1103/PhysRevLett.59.1189>.
6. D. S. Wiersma, *Nature Physics* **4**, 359 (2008), ISSN 1745-2481, URL <https://doi.org/10.1038/nphys971>.
7. A. Schilke, C. Zimmermann, P. W. Courteille, and W. Guerin, *Nature Photonics* **6**, 101 (2011), URL <https://doi.org/10.1038/nphoton.2011.320>.
8. V. S. Letokhov, *Soviet Journal of Experimental and Theoretical Physics* **26**, 835 (1968).
9. D. S. Wiersma and A. Lagendijk, *Phys. Rev. E* **54**, 4256 (1996), URL <https://link.aps.org/doi/10.1103/PhysRevE.54.4256>.
10. H. Cao, J. Xu, Y. Ling, A. Burin, E. Seeling, X. Liu, and R. Chang, *IEEE Journal of Selected Topics in Quantum Electronics* **9**, 111 (2003).
11. Z. Wang, M. Cao, G. Shao, Z. Zhang, H. Yu, Y. Chen, Y. Zhang, Y. Li, B. Xu, Y. Wang, et al., *The Journal of Physical Chemistry Letters* **11**, 767 (2020), PMID: 31934764, <https://doi.org/10.1021/acs.jpcllett.9b03409>, URL <https://doi.org/10.1021/acs.jpcllett.9b03409>.
12. S. Y. Zhu, M. O. Scully, H. Fearn, and L. M. Narducci, *Zeitschrift für Physik D Atoms, Molecules and Clusters* **22**, 483 (1992), ISSN 1431-5866, URL <https://doi.org/10.1007/BF01426090>.
13. H. Fearn, M. O. Scully, S. Y. Zhu, and M. Sargent, *Zeitschrift für Physik D Atoms, Molecules and Clusters* **22**, 495 (1992), ISSN 1431-5866, URL <https://doi.org/10.1007/BF01426091>.
14. W. Guerin, F. Michaud, and R. Kaiser, *Phys. Rev. Lett.* **101**, 093002 (2008), URL <https://link.aps.org/doi/10.1103/PhysRevLett.101.093002>.
15. G. Labeyrie, F. de Tomasi, J.-C. Bernard, C. A. Müller, C. Miniatura, and R. Kaiser, *Phys.*

- Rev. Lett. **83**, 5266 (1999), URL <https://link.aps.org/doi/10.1103/PhysRevLett.83.5266>.
16. T. Binninger, V. N. Shatokhin, A. Buchleitner, and T. Wellens, Phys. Rev. A **100**, 033816 (2019), URL <https://link.aps.org/doi/10.1103/PhysRevA.100.033816>.
 17. J. Rosato, Physical review. E, Statistical, nonlinear, and soft matter physics **87**, 043108 (2013).
 18. D. V. Kupriyanov, I. M. Sokolov, P. Kulatunga, C. I. Sukenik, and M. D. Havey, Phys. Rev. A **67**, 013814 (2003), URL <https://link.aps.org/doi/10.1103/PhysRevA.67.013814>.
 19. B. Grémaud, T. Wellens, D. Delande, and C. Miniatura, Phys. Rev. A **74**, 033808 (2006), URL <https://link.aps.org/doi/10.1103/PhysRevA.74.033808>.
 20. Q. Baudouin, W. Guerin, and R. Kaiser, in *Annual Review of Cold Atoms and Molecules* (World Scientific, 2014), chap. 5: Cold and hot atomic vapors: A testbed for astrophysics?, pp. 251–311.
 21. A. M. Akulshin, F. P. Bustos, and D. Budker, Opt. Lett. **43**, 5279 (2018), URL <https://opg.optica.org/ol/abstract.cfm?URI=ol-43-21-5279>.
 22. A. Papoyan, S. Shmavonyan, A. Khanbekyan, H. Azizbekyan, M. Movsisyan, G. Bao, D. Kanta, A. Wickenbrock, and D. Budker, Journal of Physics B: Atomic, Molecular and Optical Physics **52**, 195003 (2019), URL <https://dx.doi.org/10.1088/1361-6455/ab38e3>.
 23. E. Gazazyan, G. Grigoryan, and A. Papoyan, J. Contemp. Phys. (Arm. Acad. Sci.) **46**, 145–149 (2011).
 24. N. Cherroret, M. Hemmerling, G. Labeyrie, D. Delande, J. T. M. Walraven, and R. Kaiser, Physical Review A **104** (2021), URL <https://doi.org/10.1103/PhysRevA.104.053714>.
 25. M. Movsisyan, S. Shmavonyan, and A. Papoyan, Cent. Eur. J. Phys. **9**, 948 (2011).
 26. B. V. Zhdanov and R. J. Knize, Optical Engineering **52**, 021010 (2012), URL <https://doi.org/10.1117/1.0E.52.2.021010>.
 27. Z. Burshtein, Optical Engineering **49**, 091005 (2010), URL <https://doi.org/10.1117/1.3483907>.
 28. R. W. Boyd, M. S. Malcuit, D. J. Gauthier, and K. Rzaewski, Phys. Rev. A **35**, 1648 (1987), URL <https://link.aps.org/doi/10.1103/PhysRevA.35.1648>.
 29. G. S. Agarwal, Springer Tracts in Modern Physics **70**, 1 (1974).
 30. J. Rosato, Phys. Rev. Lett. **107**, 205001 (2011), URL <https://link.aps.org/doi/10.1103/PhysRevLett.107.205001>.

31. G. S. Agarwal, Phys. Rev. A **44**, R28 (1991), URL <https://link.aps.org/doi/10.1103/PhysRevA.44.R28>.
32. J. Mompart and R. Corbalán, Journal of Optics B: Quantum and Semiclassical Optics **2**, R7 (2000), URL <https://dx.doi.org/10.1088/1464-4266/2/3/201>.
33. B. R. Mollow, Phys. Rev. A **5**, 2217 (1972), URL <https://link.aps.org/doi/10.1103/PhysRevA.5.2217>.
34. H.-S. Chou and J. Evers, Phys. Rev. Lett. **104**, 213602 (2010), URL <https://link.aps.org/doi/10.1103/PhysRevLett.104.213602>.
35. C. Müller and T. M. Stace, Phys. Rev. A **95**, 013847 (2017), URL <https://link.aps.org/doi/10.1103/PhysRevA.95.013847>.
36. W. Chalupczak, W. Gawlik, and J. Zachorowski, Phys. Rev. A **49**, 4895 (1994), URL <https://link.aps.org/doi/10.1103/PhysRevA.49.4895>.
37. G. Grynberg and C. Cohen-Tannoudji, Optics Communications **96**, 150 (1993), ISSN 0030-4018, URL <https://www.sciencedirect.com/science/article/pii/003040189390538G>.
38. Q. Baudouin, N. Mercadier, V. Guarrera, W. Guerin, and R. Kaiser, Nature Physics **9**, 357 (2013), ISSN 1745-2481, URL <https://doi.org/10.1038/nphys2614>.
39. T. Li, R. P. Baker, and J. D. Weinstein, J. Opt. Soc. Am. B **29**, 2848 (2012), URL <https://opg.optica.org/josab/abstract.cfm?URI=josab-29-10-2848>.
40. R. W. Boyd, M. G. Raymer, P. Narum, and D. J. Harter, Phys. Rev. A **24**, 411 (1981), URL <https://link.aps.org/doi/10.1103/PhysRevA.24.411>.
41. J. Gea-Banacloche, M. O. Scully, and M. S. Zubairy, Physica Scripta **1988**, 81 (1988), URL <https://dx.doi.org/10.1088/0031-8949/1988/T21/015>.
42. G. L. Lippi, Atoms **9** (2021), ISSN 2218-2004, URL <https://www.mdpi.com/2218-2004/9/1/6>.
43. M. Blazek, S. Hartmann, A. Molitor, and W. Elsaesser, Opt. Lett. **36**, 3455 (2011), URL <https://opg.optica.org/ol/abstract.cfm?URI=ol-36-17-3455>.
44. I. V. Doronin, E. S. Andrianov, A. A. Zyablovsky, A. A. Pukhov, Y. E. Lozovik, A. P. Vinogradov, and A. A. Lisiansky, Opt. Express **27**, 10991 (2019), URL <https://opg.optica.org/oe/abstract.cfm?URI=oe-27-8-10991>.
45. H. Cao, J. Y. Xu, S.-H. Chang, and S. T. Ho, Phys. Rev. E **61**, 1985 (2000), URL <https://link.aps.org/doi/10.1103/PhysRevE.61.1985>.

46. G. Hazak and O. Zahavi, Phys. Rev. A **46**, 4261 (1992), URL <https://link.aps.org/doi/10.1103/PhysRevA.46.4261>.
47. J. C. Garrison, H. Nathel, and R. Y. Chiao, J. Opt. Soc. Am. B **5**, 1528 (1988), URL <https://opg.optica.org/josab/abstract.cfm?URI=josab-5-7-1528>.
48. R. C. Hilborn, *Einstein coefficients, cross sections, f values, dipole moments, and all that* (2002), physics/0202029.
49. D. Steck (2003).
50. A. V. Taichenachev, A. M. Tumaikin, and V. I. Yudin, **83**, 949–961 (1996), URL <http://jetp.ras.ru/cgi-bin/e/index/e/83/5/p949?a=list>.
51. F. Bustos, D. Calia, D. Budker, M. Centrone, J. Hellemeier, P. Hickson, R. Holzlöhner, and S. Rochester, Nature Commun. **9** (2018).